

Density-Matrix Mean-Field Theory

Junyi Zhang^{1, 2*} and Zhengqian Cheng³

¹ William H. Miller III Department of Physics and Astronomy, Johns Hopkins University,
Baltimore, Maryland 21218, USA

² Institute for Quantum Matter, Johns Hopkins University, Baltimore, Maryland, 21218, USA

³ Department of Applied Physics and Applied Mathematics, Columbia University, New York,
New York 10027, USA

* jzhan312@jhu.edu

April 24, 2024

Abstract

Mean-field theories have proven to be efficient tools for exploring various phases of matter, complementing alternative methods that are more precise but also more computationally demanding. Conventional mean-field theories often fall short in capturing quantum fluctuations, which restricts their applicability to systems characterized by strong quantum fluctuations. In this article, we propose a novel mean-field theory, density-matrix mean-field theory (DMMFT). DMMFT constructs effective Hamiltonians, incorporating quantum environments shaped by entanglements quantified by the reduced density matrices. Therefore, it offers a systematic and unbiased approach to account for effects of fluctuations and entanglements in quantum ordered phases. As demonstrative examples, we show that DMMFT can not only quantitatively evaluate the renormalization of order parameters induced by quantum fluctuations but can even detect the topological order of quantum phases. Additionally, we discuss the extensions of DMMFT for systems at finite temperatures and those with disorders. Our work provides a novel and efficient approach to explore phases exhibiting unconventional quantum orders, which can be particularly beneficial for investigating frustrated spin systems in high spatial dimensions.

Contents

1	Introduction	2
2	Density-Matrix Mean-Field Theory	4
2.1	Conventional Mean-Field Approximation	4
2.2	Density-Matrix Mean-Field Approximation	6
2.3	Comparison of the Mean-Field Approximations	7
3	Applications	8
3.1	Affleck-Kennedy-Lieb-Tasaki Model	9
3.2	Antiferromagnetic Heisenberg Model on Triangular Lattices	10
4	Discussions	14
4.1	Comparisons with Alternative Methods	14
4.1.1	Comparison with Density-Matrix Renormalization Group	14
4.1.2	Comparison with Dynamical Mean-Field Theory	15

4.1.3	Comparison with Cluster Variation Method	16
4.1.4	Comparison with Linked-Cluster Expansion	17
4.2	Systems at Finite Temperatures	17
4.3	Systems with Disorders	18
5	Conclusion	19
A	Iterative Algorithm for Mean-Field Equations	19
B	Pseudocodes for Heisenberg Model	20
	References	23

1 Introduction

Frustrated Hubbard and Heisenberg models [1–3] have continued to capture research attention over the last half-century due to their potential to host various intriguing quantum phases [4–8], as well as their relevance to high T_c superconductors [9] and their applications in quantum computations [10]. Determining the ground states of frustrated Hubbard and Heisenberg models is often a challenging task.

Exact approaches frequently encounter limitations posed by the exponential wall. In exact diagonalization (ED), the dimension of the Hilbert space increases exponentially with the system size. In density-matrix renormalization group (DMRG) [11], the area law provides relief from the exponential wall issue for gapped systems in one spatial dimension ($d = 1$), it still faces exponential scaling challenges for gapless systems or in higher dimensions ($d \geq 2$) [12–14]. On the other hand, quantum Monte Carlo (QMC) methods are less constrained by the system size. Nevertheless, the notorious sign problem often plagues fermionic systems and frustrated magnetic systems [15, 16].

Approximation methods, serving as complements to exact approaches, prove to be useful and efficient tools for exploring various phases of a system. Conventional mean-field theories (MFTs) already provide insights into non-trivial effects arising from the interactions, e.g., the formation of the local moments in metals [17], and the BCS theory for the superconductivity [18]. Conventional MFTs achieve the simplification by neglecting the fluctuations, consequently, they tend to exhibit bias towards ordered states and overlook the nuanced effects stemming from the fluctuations.

Beyond conventional MFTs, various approximations have been proposed for fermionic systems [19–25]. In dynamical mean-field theory (DMFT), a lattice model is mapped to a local impurity model, and the effective action is constructed using Green’s functions as dynamical mean fields [19], which allows DMFT to capture the quantum features of the metal-insulator transitions [20]. While DMFT precisely describes systems in infinite dimensions, the computational demands of solving the local impurity problems with continuous baths necessitate ongoing efforts to further simplify the DMFT. Recently, a quantum embedding method called density matrix embedding theory (DMET) has been introduced to enhance the efficiency of the DMFT by taking the advantage of the frequency-independent local density matrix [21]. More recently, another simplification of DMFT known as variational discrete action theory (VDAT) has also been proposed utilizing sequential product density matrix to variationally determine ground states [22–25].

Despite of the successes of DMFT and its simplifications for fermionic systems, a gap remains in methods beyond semiclassical mean-field approximations for spin systems. Although employing the Holstein-Primakoff transformation [26] allows spins to be mapped to bosons, to which the DMFT may be adapted in principle, the transformation is nonlinear, and the semiclassical large- S expansion becomes less controllable for $S = 1/2$ in the quantum limit, posing challenges for semiclassical methods applied to quantum spins. Similar challenges may be encountered with alternative methods. For instance, in Schwinger boson representation [27], one needs to set $\mathcal{N} = 2$ for the quantum limit after a saddle-point mean-field approximation with large \mathcal{N} .

In this article, we propose a new mean-field method beyond conventional MFTs, which we call density-matrix mean-field theory (DMMFT). DMMFT constructs effective Hamiltonians, incorporating quantum environments shaped by entanglements quantified by the reduced density matrices without presumed semiclassical orders. Therefore, it offers an unbiased approach to account for effects of fluctuations and entanglements in quantum ordered phases. In contrast to QMC and DMFT, DMMFT is generically applicable to systems of fermions, bosons as well as spins, regardless of frustrations. More importantly, by gauging the quantum fluctuations with the reduced DM, DMMFT can detect not only the symmetry-breaking phases in Landau's paradigm but also the topological phases with the help of entanglement spectra. Our work provides a novel and efficient approach to explore phases exhibiting unconventional quantum orders. Particularly, it fills the gap left by the MFTs in studying quantum ordered phases in frustrated spin systems, where semiclassical methods become less controllable in the quantum limit, and QMC methods fail due to the sign problem.

Regarding DMMFT as a generalized cluster MFT, it is also worth noticing that there are alternative cluster based methods used for studying quantum spin systems, such as the cluster variation method (CVM) and the linked-cluster expansion (LCE). Following Kikuchi's early study of the Ising model using [28], the CVM has also been extended for studying the quantum Heisenberg models [29–31]. CVM decomposes the entropic contribution to the free energy in terms of the cluster entropies that depends only on the reduced DM over the clusters. It becomes precise if the clusters up to the size of the entire system are considered [32]. CVM provides a systematic framework analyzing various cluster mean-field approximations as demonstrated in Ref. 29. Examined from the perspective of CVM, DMMFT includes the high-order cluster corrections containing essential information of quantum fluctuations beyond conventional MFTs. Similarly, LCE also decomposes the corrections to the physical observables into a series of terms depending on the clusters [33–38]. An early development of the LCE treats the expansion of the free energy perturbatively in temperature, therefore it only performs well at high temperatures [33–35]. Improvement has been made by extending LCE for calculating cluster physical observables unperturbatively in temperature, also known as numerical LCE [36–38], which has been applied to some interesting frustrated quantum magnets [39,40]. Complementing LCE below the critical temperature where long-range order develops, DMMFT does not suffer from convergence problems and can be more computationally efficient, as it does not require summation over a large number of clusters.

The rest of the article is organized as follows. In Sec. 2, we present the generic formulation of the DMMFT. The mean-field equations of DMMFT are derived in parallel to those of conventional MFTs. Moreover, we demonstrate that DMMFT becomes equivalent to conventional MFTs when the hyperparameter that gauges the quantum fluctuations is minimized. In Sec. 3, we apply the DMMFT to two demonstrative examples, 1) the Affleck-Khomoto-Lieb-Tasaki (AKLT) model [41–43], and 2) the antiferromagnetic Heisenberg model on triangular lattices (AFHTL) [44–58]. (Cf. Ref. 50 and references therein for a more comprehensive introduction to the frustrated Heisenberg models.) In the AKLT model, DMMFT is able to identify the topological ground states through their entanglement spectra. In the AFHTL, DMMFT reveals

that quantum fluctuations not only renormalize the order parameters but also shift the phase boundaries. In Sec. 4, we compare DMMFT with DMRG and DMFT, as well as the cluster-based methods, CVM and LCE. Additionally, we discuss the extensions of DMMFT for systems at finite temperatures and those with disorders. In Sec. 5, we draw conclusions and discuss potential avenues for future research. To aid readers in understanding and applying DMMFT, appendices formulating the iterative algorithm for solving DMMFT equations and the pseudocodes implementing DMMFT for the AFHTL are presented in Append. A and B, respectively.

2 Density-Matrix Mean-Field Theory

In this section, we formulate the DMMFT for a generic Hamiltonian. Let $\mathcal{I} = \{i\}$ be a set of all sites. On each site, there is a collection of local operators $\mathcal{O}_i = \{O_i^\alpha\}$. A generic Hamiltonian of local operators can be organized as follows

$$H[\mathcal{O}_{\mathcal{I}}] = \sum_{c \in \mathcal{C}} H_c[\mathcal{O}_c] + \sum_{(c,c')} H_{c,c'}[\mathcal{O}_c, \mathcal{O}_{c'}] + \sum_{(c,c',c'')} H_{c,c',c''}[\mathcal{O}_c, \mathcal{O}_{c'}, \mathcal{O}_{c''}] + \dots, \quad (1)$$

where $\mathcal{C} = \{c\}$ is a partition of \mathcal{I} , and $\mathcal{O}_{\mathcal{S}} = \cup_{i \in \mathcal{S}} \mathcal{O}_i$ is the collection of local operators over the sites within a set \mathcal{S} . In Eq.(1), H_c depends only on the local operators within a cluster c , while $H_{c,c'}, H_{c,c',c''}, \dots$ describe the inter-cluster couplings. For systems with finite-range interactions, there are proper partitions such that interactions only involve finitely many clusters.

Conventional MFTs isolate a local cluster from the system and coupled to an effective environment, where the environment is assumed to be classical, and the correlated fluctuations between the cluster and the environment are neglected. DMMFT improves the conventional mean-field approximation by including the essential quantum fluctuations in the environment, where the reduced DM is used to gauge the quantum fluctuations and select a Hilbert subspaces approximating the effective environment. In this section, we shall formulate DMMFT for the Hamiltonian in Eq.(1) without further assumptions specifying the local operators or the microscopic details of the coupling terms, therefore DMMFT is a method generically applicable to fermions, bosons as well as spins, irrespective of the presence of frustrations.

In the following subsections, we begin by reviewing the conventional mean-field approximation in Sec. 2.1. Then, we develop the mean-field equations and self-consistency conditions of DMMFT in parallel to those in conventional MFTs in Sec. 2.2. Following this, in Sec. 2.3, we conduct a comprehensive comparison between the DMMFT and the conventional MFTs. Within this comparison, we identify a hyperparameter, n_c , that interpolates the DMMFT and the conventional MFTs. Particularly, when $n_c = 1$, attaining its minimal value, DMMFT becomes equivalent to the conventional MFTs.

2.1 Conventional Mean-Field Approximation

We review the approximations employed in conventional MFTs before delving into the development of DMMFT. In conventional MFTs, the mean-field decoupling localizes the operator products to individual Hilbert subspaces by neglecting the correlated fluctuations. More precisely, consider an operator product $O_i^\alpha O_j^\beta$ acting on the Hilbert space $\mathcal{H}_i \otimes \mathcal{H}_j$. The conventional mean-field approximation decouples the operator product as follows

$$O_i^\alpha O_j^\beta \approx O_i^\alpha \langle O_j^\beta \rangle + \langle O_i^\alpha \rangle O_j^\beta - \langle O_i^\alpha \rangle \langle O_j^\beta \rangle, \quad (2)$$

where the terms on the right-hand side act on the subspace \mathcal{H}_i or \mathcal{H}_j , or act trivially as an additive c -number. Consequently, the correlated fluctuations $\langle \delta O_i^\alpha \delta O_j^\beta \rangle = \langle O_i^\alpha O_j^\beta \rangle - \langle O_i^\alpha \rangle \langle O_j^\beta \rangle$ vanish in this approximation. Alternatively, from the perspective of the quantum states, as the operator product factorizes in product states, $\langle \phi_i | \otimes \langle \phi_j | O_i^\alpha O_j^\beta | \phi_i \rangle \otimes | \phi_j \rangle = \langle \phi_i | O_i^\alpha | \phi_i \rangle \langle \phi_j | O_j^\beta | \phi_j \rangle$,

the conventional MFTs implicitly assume the product structure of the states and neglect quantum entanglements.

Keeping this consideration in mind, we formulate the conventional mean-field approximation for the generic Hamiltonian in Eq.(1) as follows. Given a cluster c , let $\mathcal{C}'_c = \cup c'$ be the collection of the cluster connecting to c , referred to as the environment surrounding c . The associated Hilbert spaces are \mathcal{H}_c and $\mathcal{H}_{\mathcal{C}'_c}$ for the cluster and the environment, respectively, where $\mathcal{H}_{\mathcal{S}} = \otimes_{i \in \mathcal{S}} \mathcal{H}_i$ for a set of sites \mathcal{S} . Retaining the terms within the extended cluster $\bar{c} = c \cup \mathcal{C}'_c$, the local Hamiltonian is

$$\begin{aligned} H[\mathcal{O}_{\bar{c}}] &= H_c[\mathcal{O}_c] + H_{c,\mathcal{C}'_c}[\mathcal{O}_c, \mathcal{O}_{\mathcal{C}'_c}] + H_{\mathcal{C}'_c}[\mathcal{O}_{\mathcal{C}'_c}], \\ H_{c,\mathcal{C}'_c}[\mathcal{O}_c, \mathcal{O}_{\mathcal{C}'_c}] &= \sum_{(c,c'):c' \in \mathcal{C}'_c} H_{c,c'}[\mathcal{O}_c, \mathcal{O}_{c'}] + \sum_{(c,c',c''):c',c'' \in \mathcal{C}'_c} H_{c,c',c''}[\mathcal{O}_c, \mathcal{O}_{c'}, \mathcal{O}_{c''}] + \dots, \\ H_{\mathcal{C}'_c}[\mathcal{O}_{\mathcal{C}'_c}] &= \sum_{c' \in \mathcal{C}'_c} H_{c'}[\mathcal{O}_{c'}] + \sum_{(c',c''):c',c'' \in \mathcal{C}'_c} H_{c',c''}[\mathcal{O}_{c'}, \mathcal{O}_{c''}] + \dots, \end{aligned} \quad (3)$$

where H_c is the Hamiltonian of the focused cluster c , $H_{\mathcal{C}'_c}$ is the Hamiltonian of the environment \mathcal{C}'_c , and H_{c,\mathcal{C}'_c} represents the couplings between the cluster c and its environment \mathcal{C}'_c . If the target state can be approximated by a product state locally, i.e.,

$$|\phi_{\bar{c}}\rangle \approx |\phi_{\bar{c}}^{\text{MF}}\rangle = |\phi_c\rangle \otimes |\phi_{\mathcal{C}'_c}\rangle, \quad (4)$$

a local effective Hamiltonian for the cluster c can be obtained by substituting the operators over $\mathcal{H}_{\mathcal{C}'_c}$ with their expectation values in $|\phi_{\mathcal{C}'_c}\rangle$, i.e.,

$$H_{\text{MF}}^{(c)}[\mathcal{O}_c] = H_c[\mathcal{O}_c] + \langle \phi_{\mathcal{C}'_c} | H_{c,\mathcal{C}'_c}[\mathcal{O}_c, \mathcal{O}_{\mathcal{C}'_c}] | \phi_{\mathcal{C}'_c} \rangle + \langle \phi_{\mathcal{C}'_c} | H_{\mathcal{C}'_c}[\mathcal{O}_{\mathcal{C}'_c}] | \phi_{\mathcal{C}'_c} \rangle, \quad (5)$$

which acts only on the Hilbert subspace \mathcal{H}_c . One solves $|\phi_c\rangle$ as an eigenstate with respect to the effective Hamiltonian $H_{\text{MF}}^{(c)}$ for each cluster c locally. If one further assumes that the target state of the entire system can also be approximated with a product state, i.e.,

$$|\Phi_{\text{MF}}\rangle = \otimes_c |\phi_c\rangle, \quad (6)$$

then, for each extended cluster, $|\phi_{\bar{c}}\rangle = \otimes_{c' \in \mathcal{C}'_c} |\phi_{c'}\rangle$. Therefore, Eq.(4), Eq.(5), and Eq.(6) form a closed set of coupled mean-field equations for the conventional MFTs.

The mean-field equations can often be further simplified when systems have additional symmetries. If the partition $\mathcal{C} = \{c\}$ respects some symmetries of the system, there exist symmetry transformations relating the clusters $T_{c',c} : c \mapsto c'$. A symmetric mean-field Ansatz state can be constructed simply as $|\Phi_{\text{MF}}\rangle = \otimes_c T_{c,c_0} |\phi_{c_0}\rangle$. Particularly, for a translationally invariant state, all $|\phi_c\rangle$ can be chosen equal to the same state $|\phi_{c_0}\rangle$ in the local Hilbert space \mathcal{H}_{c_0} , then the coupled mean-field equations for the clusters reduce to a single set of self-consistent mean-field equations for $|\phi_{c_0}\rangle$.

The major assumption in the conventional MFTs described above is that the target states can be approximated with product states [Eqs.(4) and (6)], which is, nevertheless, not justified *a priori*. For many ordered states, the correlated fluctuations arising from the quantum entanglements are not negligible, particularly at short range. Prototypically, in frustrated magnetic systems and symmetry-protected topologically ordered systems, such quantum fluctuations and quantum entanglements play essential roles. Improved treatments of quantum fluctuations and quantum entanglements are needed to better understand the emerging quantum ordered phases.

2.2 Density-Matrix Mean-Field Approximation

The simplifications achieved in conventional MFTs stem from the *separability*, i.e., reducing the challenging task of studying the total Hamiltonian H over an exponentially large Hilbert space \mathcal{H}_c to the more manageable tasks of studying the local Hamiltonians $H_{\text{MF}}^{(c)}$ over local \mathcal{H}_c . However, it is not *necessary* for a system to be in a product state for two local subsystems to be separable. The assumptions of the product states [Eqs.(4) and (6)] can thus be relaxed. More precisely, for gapped systems, the correlated fluctuations $\langle \delta O_i^\alpha \delta O_j^\beta \rangle \rightarrow 0$ as $|i-j| \rightarrow \infty$. The absence of long-range entanglements ensures separability, allowing the local physics to be approximated with effective local systems. However, the short-range entanglements encode the quantum fluctuations, demanding a more faithful treatment.

Instead of Eq.(2) for mean-field decoupling, it is instructive to recognize that the entanglement of a local cluster with an (infinite or finitely large) environment can always be *faithfully* reproduced within a finite extension of the cluster. More precisely, consider a generic state $|\Psi\rangle \in \mathcal{H}_c$. The entanglement of the state $|\Psi\rangle$ over the cluster c and the rest parts of the system $\mathcal{C}\setminus c$ can be characterized by the reduced DM

$$\rho_c = \text{Tr}_{\mathcal{C}\setminus c} |\Psi\rangle\langle\Psi|. \quad (7)$$

The entanglement is controlled by \mathcal{H}_c than $\mathcal{H}_{\mathcal{C}\setminus c}$ provided $D_{\mathcal{H}_c} < D_{\mathcal{H}_{\mathcal{C}\setminus c}}$, where $D_{\mathcal{H}}$ denotes the dimension of the Hilbert space \mathcal{H} . According to the purification theorem [59], there exists a state $|\tilde{\Psi}\rangle$ in $\tilde{\mathcal{H}} = \mathcal{H}_c \otimes \tilde{\mathcal{H}}_{\bar{c}}$ such that $\text{Tr}_{\tilde{\mathcal{H}}}\langle\tilde{\Psi}|\langle\tilde{\Psi}| = \tilde{\rho}_c$ is equivalent to ρ_c , and the dimension of the Hilbert subspace $\tilde{\mathcal{H}}_{\bar{c}}$ is bounded by $\tilde{D}_{\bar{c}}^E = \lceil \exp(SE_c) \rceil$, where

$$SE_c = -\text{Tr}_c [\rho_c \ln(\rho_c)], \quad (8)$$

is the entanglement entropy and $\lceil q \rceil$ represents the smallest integer larger than or equal to q . In this context, DMMFT seeks for an effective Hamiltonian $\tilde{H}_{\text{MF}}^{(c)}$ over some $\tilde{\mathcal{H}}$ (to be specified below), such that the reduced DM of the state obtained from the the Hamiltonian,

$$\rho_c^{\text{MF}} = \text{Tr}_{\tilde{\mathcal{H}}}\langle\tilde{\Phi}|\langle\tilde{\Phi}|, \quad (9)$$

well approximates the reduced DM of the target state $\rho_c = \text{Tr}_{\mathcal{C}\setminus c} |\Phi\rangle\langle\Phi|$.

Instead of Eq.(4), DMMFT assumes that *for systems without long-range entanglements*, $\tilde{\mathcal{H}}$ can be found as a Hilbert subspace of $\mathcal{H}_{\bar{c}}$ over the extended cluster \bar{c} . Mathematically, there exists a homomorphism

$$\Pi = \text{Id}_c \otimes \Pi_{\mathcal{C}'_c} : \tilde{\mathcal{H}} \rightarrow \mathcal{H}_{\bar{c}}, \quad (10)$$

and its pseudo-inverse $\Pi^\dagger : \mathcal{H}_{\bar{c}} \rightarrow \tilde{\mathcal{H}}$ is a projector.

To avoid confusion, it is essential to emphasize that the $\tilde{\mathcal{H}}$ constructed in DMMFT differs from that in DMET. The purification theorem only ensures the existence of $\tilde{\mathcal{H}}$ with its dimension bounded by $\tilde{D}_{\bar{c}}^E$ from below. In DMET, an optimal \tilde{H} with the lowest possible dimension is employed, but at the cost of a less straightforward construction of the embedding Hamiltonian. In contrast, DMMFT can intuitively construct an effective Hamiltonian by restricting the Hamiltonian for the extended cluster to $\tilde{\mathcal{H}}$, i.e.,

$$\tilde{H}_{\text{MF}}^{(c)}[\mathcal{O}_c, \tilde{\mathcal{O}}_{\mathcal{C}'_c}] = \Pi^\dagger H[\mathcal{O}_{\bar{c}}] \Pi, \quad (11)$$

where the local operators in $\tilde{\mathcal{O}}_{\mathcal{C}'_c}$ are

$$\tilde{\mathcal{O}}_j^\beta = \Pi_{\mathcal{C}'_c}^\dagger \mathcal{O}_j^\beta \Pi_{\mathcal{C}'_c}, \forall j \in \mathcal{C}'_c. \quad (12)$$

The reduced density matrix of the target state is approximated with ρ_c^{MF} [Eq.(9)] for an eigenstate $|\tilde{\phi}\rangle$ of $\tilde{H}_{\text{MF}}^{(c)}$.

Reciprocally, for each ρ_c , we may construct the local projectors Π_c as follows. Let $\{\lambda_i^{(c)}, |\lambda_i^{(c)}\rangle\}$ be the spectral decomposition of ρ_c , and assume the state vectors are arranged in decreasing order according to their eigenvalues, i.e., $\lambda_i^{(c)} \geq \lambda_j^{(c)}, \forall i < j$. Define

$$\Pi_c = \sum_{i=1}^{n_c} |\lambda_i^{(c)}\rangle\langle\lambda_i^{(c)}|, \quad (13)$$

where $n_c \leq D_{\mathcal{H}_c}$ is a cut-off parameter. For the extended cluster $\bar{c} = c \cup C'_c$, we choose

$$\Pi_{C'_c} = \otimes_{c' \in C'_c} \Pi_{c'}. \quad (14)$$

Parallel to the mean-field equations for the conventional MFTs, Eqs.(9) – (14) constitute a closed set of coupled mean-field equations for the DMMFT. In the presence of symmetries, the mean-field equations can be further simplified. Specifically, for a translationally invariant target state $|\Phi\rangle$, the reduced DMs of the local clusters are all identical to the same reduced DM ρ_{c_0} (so are the projectors). Consequently, the coupled mean-field equations for the clusters reduce to a single set of self-consistent mean-field equations for ρ_{c_0} . The procedures for implementing the DMMFT algorithm are outlined in the Appendices.

2.3 Comparison of the Mean-Field Approximations

Comparing conventional MFTs with DMMFT, we find the cut-off parameter n_c in Eq.(13) can be regarded as a hyperparameter interpolating the DMMFT and the conventional MFT. To demonstrate this point, we first observe that when $D_{\mathcal{H}_{C'_c}} = 1$, DMMFT is equivalent to a conventional MFT. If the ground state is a product state [Eq.(6)], the local reduced DM of cluster c is $\rho_c = |\phi_c\rangle\langle\phi_c|$. The expectation values of the local observables agree

$$\langle O_i^\alpha \rangle_c = \langle \phi_c | O_i^\alpha | \phi_c \rangle = \text{Tr}_c(\rho_c O_i^\alpha). \quad (15)$$

Moreover, since $\Pi = \text{Id}_c \otimes (\otimes_{c'} |\phi_{c'}\rangle\langle\phi_{c'}|)$, $\tilde{\mathcal{H}}$ is isomorphic to \mathcal{H}_c , and the effective Hamiltonians $\tilde{H}_{\text{MF}}^{(c)}$ are $H_{\text{MF}}^{(c)}$ identical under this isomorphism.

Furthermore, from Eq.(14), we have $D_{\mathcal{H}_{C'_c}} = \prod_{c' \in C'_c} n_{c'}$. Therefore, we may take n_c as a hyperparameter interpolating the conventional MFT and the DMMFT. When $n_c = 1$ (set to its minimal value), the DMMFT simply reduces to the conventional MFT, which underestimates the quantum fluctuations. When $n_c = D_{\mathcal{H}_c}$ (set to its maximal value), the DMMFT describes a collection of (overlapped) extended cluster \bar{c} , which overestimate the quantum fluctuations compared to the infinite system in the thermodynamic limit. Therefore, as n_c increases from 1 to $D_{\mathcal{H}_c}$, more and more quantum fluctuations are included.

Since n_c gauges the amount of quantum fluctuations included in DMMFT from underestimation to overestimation, it seems reasonable to expect an optimal choice of its value, which leads to the following *conjecture*.

Conjecture. *The optimal choice of the hyperparameters is given by*

$$n_c^* = \tilde{D}_c^E = \lceil \exp(SE_c) \rceil. \quad (16)$$

We do not have a mathematical proof of this conjecture, which nevertheless will not harm the practicality of the DMMFT. Particularly, one may take $n_c = \tilde{D}_c^E$ as a rule-of-thumb choice and treat n_c as a *variational* hyperparameter.

It is easy to observe that ρ_c generically has non-vanishing entanglement entropy whenever $D_{\mathcal{H}_{c'}} > 1$. This is exactly the short-range entanglement captured by the DMMFT beyond the conventional MFTs. Not surprisingly, one expects that the DMMFT may detect short-range entangled topological phases with a properly chosen n_c . In Sec. 3.1, we demonstrate with the AKLT model that DMMFT can indeed detect the topological ground states in terms of the entanglement spectra without being biased to the symmetry-breaking states.

Lastly, we comment on the separability in DMMFT. In contrast to Eq.(6) for the conventional MFTs, DMMFT does not assume the product structure of the state. Instead, the weaker version of the separability adopted by DMMFT is

$$\rho_{c_1, c_2}^{(2)} = \text{Tr}_{\mathcal{C} \setminus (c_1 \cup c_2)} |\Phi\rangle\langle\Phi| \approx \rho_{c_1} \otimes \rho_{c_2}, \quad (17)$$

for any two clusters c_1 and c_2 that are not connected.

3 Applications

In this section, we apply the DMMFT to two demonstrative examples, the AKLT model and the AFHTL, that have been extensively studied in the literatures. The AKLT model was historically proposed as an exactly solvable model to confirm Haldane's conjecture regarding antiferromagnetic spin-1 chains [41–43]. We choose the AKLT model as our illustrative example not solely because of its exact solvability but primarily due to its intriguing property that the expectations of local moments, and consequently the usual Néel order parameter (alternating magnetization), vanish in the ground states [42, 43]. This property challenges the ability of conventional MFTs to detect the orders borne in the ground states of the AKLT model. Moreover, despite proposals suggesting that topological orders in one dimension can be characterized by nonlocal order parameters, such as string order [60], it is still desirable to identify local features that can distinguish topologically ordered states from disordered or trivially ordered states, especially at the mean-field level. In Sec. 3.1, we demonstrate that DMMFT can correctly detect the topological ground states based on the reduced DM and the entanglement spectra. All local observables that can serve as an order parameter can be simply calculated with respect to the reduced DM according to Eq.(15). Nevertheless, the entanglement spectra reveal additional information beyond conventional MFTs, reflecting the quantum nature of orders. It should be emphasized that the topological order in the ground states of the AKLT model is a generic feature of this exotic phase, which is not restricted to the integrable point of the AKLT model, but persists upon perturbations that do not close the gap. The exact solvability of the AKLT model here only serves as a convenient benchmark allowing quantitative comparisons.

The AFHTL serves as a prototypical model representing frustrated magnetisms. Inspired by the pioneering study of Fazekas and Anderson's [5], it has been proposed that various intriguing phases are potentially hosted by the AFHTL due to the frustrations [6, 14, 61–67]. In Sec. 3.2, we apply the DMMFT to the simplest case of the AFHTL, which includes only the nearest-neighbor couplings and the easy-axis anisotropy. Even in this simplest case, the ground state of the system exhibits a noncollinear three-sublattice order, reminiscent of the semiclassical Néel state. However, the order parameters are subjected to significant renormalization due to cooperative interactions between quantum fluctuations and frustration-induced noncollinearity [44–46]. Furthermore, we also report the magnetization of the AFHTL in a longitudinal magnetic field, which has been extensively studied in literatures, both in classical and quantum contexts [47–57]. Particularly, it has been noted that the quantum fluctuations play non-trivial roles in stabilizing the ordered states in AFHTL [56–58]. For quantitative comparison, we compute the magnetization curve using the state-of-the-art technique DMRG. Our

DMMFT results exhibit good agreement with DMRG. It should be emphasized that the simple AFHLL with only nearest-neighbor couplings and easy-axis anisotropy in a longitudinal external magnetic field makes it a robust candidate for benchmarking purposes because it has been extensively studied using various methods and confirmed in the literatures. Nevertheless, DMMFT is not solely restricted to the simple AFHLL. It can indeed also detect the stripe phases in J_1 - J_2 AFHLL [14], and the resonating valence bond phases with dimerized spins [5]. We would highlight DMMFT as a generic unbiased approach to characterizing diverse phases with classical as well as quantum orders.

3.1 Affleck-Kennedy-Lieb-Tasaki Model

We apply the DMMFT to the AKLT model. The AKLT model is a one-dimensional spin-1 chain defined by the Hamiltonian

$$H_{\text{AKLT}} = \sum_i P_{i,i+1}^{(S=2)} = \sum_i \frac{1}{2} [\mathbf{S}_i \cdot \mathbf{S}_{i+1} + \beta (\mathbf{S}_i \cdot \mathbf{S}_{i+1})^2 + \gamma], \quad (18)$$

where β describes the biquadratic coupling and γ is an additive constant, \mathbf{S}_i are spin-1 operators whose representations in the S^z -basis are

$$S_i^x = \frac{1}{\sqrt{2}} \begin{pmatrix} 0 & 1 & 0 \\ 1 & 0 & 1 \\ 0 & 1 & 0 \end{pmatrix}, S_i^y = \frac{1}{\sqrt{2}} \begin{pmatrix} 0 & -i & 0 \\ i & 0 & -i \\ 0 & i & 0 \end{pmatrix}, S_i^z = \begin{pmatrix} 1 & 0 & 0 \\ 0 & 0 & 0 \\ 0 & 0 & -1 \end{pmatrix}. \quad (19)$$

The coefficients β and γ are determined by the condition that each term in the Hamiltonian is a projector to the Hilbert subspace of total spin $S = 2$. More precisely, when $\beta = 1/3$, and $\gamma = 2/3$,

$$P_{i,i+1}^{(S=2)}(x) = \frac{1}{2}(x + \beta x^2 + \gamma) = \begin{cases} 1, & x = 1, \\ 0, & x = -1, -2. \end{cases} \quad (20)$$

where $x = \mathbf{S}_i \cdot \mathbf{S}_{i+1} = 1, -1, -2$ in total spin sectors $\mathcal{H}_{\{i,i+1\}}^{(S=2,1,0)}$ respectively. By construction, H_{AKLT} describes antiferromagnetic nearest neighbor couplings penalizing only on neighboring spins being in $S = 2$ states.

The AKLT model is an exactly solvable system, showcasing non-trivial topological order. Notably, it features spin-1/2 (fractional to spin-1) edge states and exhibits a 4-fold degeneracy of the ground states for an open chain [43], which persists even for $\beta < \frac{1}{3}$ deviating from its integrable point, provided the gap does not close [60, 68]. Moreover, the Néel order vanishes in the ground states. Therefore, the conventional MFTs fail to distinguish it from a trivial paramagnetic phase. Nevertheless, with the help of reduced DM and entanglement spectra, DMMFT is able to probe the topological order borne in its ground state.

Let us consider a two-site cluster c situated in the bulk of an infinite chain. By translational symmetry, any two-site cluster c within the chain shares the same reduced DM $\rho_c^{(2)}$. The spectrum of the two-site reduced DM is exactly known and given by $\text{eig} \rho_c^{(2)} = \{\frac{1}{3}, \frac{2}{9}, \frac{2}{9}, \frac{2}{9}, 0, 0, 0, 0, 0\}$. Furthermore, if we trace out one of the sites within the cluster, we obtain the single-site reduced DM whose spectrum is exactly known, $\text{eig} \rho_c^{(1)} = \{\frac{1}{3}, \frac{1}{3}, \frac{1}{3}\}$.

We apply the DMMFT to the AKLT model, focusing on the two-site cluster c and solving the reduced DM $\rho_c^{(2)}$ self-consistently according to the mean-field equations as described in Sec. 2.2. Specifically, the reduced DM is calculated over an extended cluster encompassing the left and right nearest-neighboring two-site clusters to c . The associated Hilbert space is denoted as $\tilde{\mathcal{H}}_c = \tilde{\mathcal{H}}_l \otimes \mathcal{H}_c \otimes \tilde{\mathcal{H}}_r$, where $\tilde{\mathcal{H}}_{l,r} \sim \Pi_c(\mathcal{H}_c)$ are the Hilbert subspaces selected by the reduced DM, as per Eq.(13). We choose the cut-off parameter $n_c = 4$.

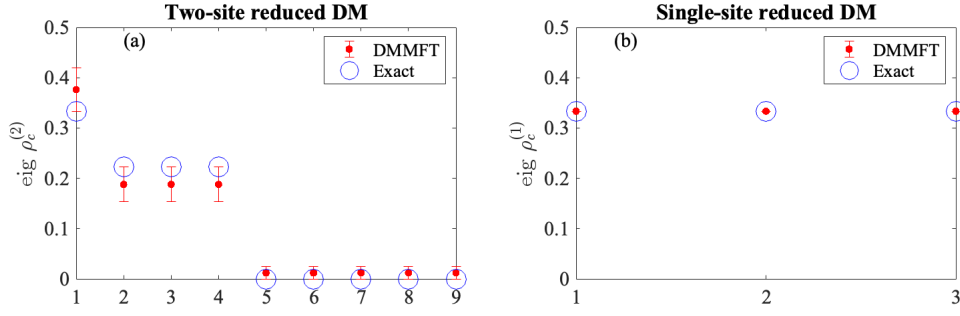


Figure 1: Spectra of the two-site and single-site reduced DMs for the AKLT model. Blue circles denote exact values, while red dots with error bars represent DMMFT results.

In Fig. 1, the spectra of the two-site and single-site reduced DMs are presented. Blue circles represent the exact values, while red dots depict the DMMFT results. The spectrum of the two-site reduced DM obtained with the DMMFT reasonably aligns with the exact values [Fig. 1(a)], notably capturing the correct degeneracies. The entanglement entropy of the two-site cluster evaluated by DMMFT is $SE_{c,\text{MF}}^{(2)} = 1.58$. Although it is slightly larger than the exact value $SE_{c,\text{exact}}^{(2)} = 1.3689$, this discrepancy is expected due to the cut-off parameter n_c chosen being marginally larger than $\exp(SE_{c,\text{exact}}^{(2)}) = 3.9310$. Fig. 1(b) displays the spectrum of the single-site reduced DM, where the DMMFT results align excellently with the exact values. The single-site entanglement entropy $SE_c^{(1)} = 1.0986 = \ln(3)$ also matches. Furthermore, the expectation values of two spins within the cluster $\langle S_{1,2}^\alpha \rangle = \text{Tr}_c(S_{1,2}^\alpha \rho_c)$ both vanish. This implies that the ground states found by DMMFT are not biased towards the semiclassical Néel states, which agrees with the exact results.

3.2 Antiferromagnetic Heisenberg Model on Triangular Lattices

We apply the DMMFT to another illustrative example, the simple AFHTL. The Hamiltonian for the AFHTL involving nearest-neighbor anisotropic exchange interactions is given by

$$\begin{aligned} H_{AFH} &= \sum_{(i,j)} \left[J_{xy} \left(S_i^x S_j^x + S_i^y S_j^y \right) + J_z S_i^z S_j^z \right] \\ &= \sum_{(i,j)} J \left[\mathcal{A} \left(S_i^x S_j^x + S_i^y S_j^y \right) + S_i^z S_j^z \right], \end{aligned} \quad (21)$$

where J_z and J_{xy} are strengths of longitudinal and transverse exchange interactions. For antiferromagnetic couplings, it is more convenient to parameterize the model with $J = J_z > 0$ and $\mathcal{A} = J_{xy}/J_z$. The phases of the system only depend on the dimensionless parameter \mathcal{A} that specifies the exchange anisotropy. Our focus is on the easy-axis case, i.e., $0 \leq \mathcal{A} \leq 1$. The two limiting points of \mathcal{A} are: 1) $\mathcal{A} = 0$, where the transverse exchange terms vanish (often referred to as the Ising limit), and 2) $\mathcal{A} = 1$, where the exchange interactions have full rotational symmetry (often referred to as the Heisenberg limit). Both limits have been extensively studied in the literatures. Particularly, in the Ising limit, quantum fluctuations are additionally introduced by the transverse magnetic field, and the sign problem of the diagonal (longitudinal) frustrations can be mitigated in the QMC simulations [58, 69]. Meanwhile, in the Heisenberg limit, the system orders in the so-called 120° -Néel state, as confirmed by various numerical methods [44–46].

While the phase diagram of the AFHTL in a longitudinal external magnetic field is believed to be bounded by the Ising and Heisenberg limits for a generic anisotropy parameter $0 < \mathcal{A} < 1$, computing the details of quantum phases remains challenging, particularly due to the QMC sign problem when $\mathcal{A} \neq 0$. In previous studies such as those in Refs. 52, 53, the magnetization has been examined using large-size cluster mean-field theory (belonging to the class of conventional MFTs) with a scaling scheme. Additionally, Ref. 47 and Ref. 49 have reported studies of the magnetization with ED, respectively, and Ref. 48 has presented phase diagram obtained with DMRG¹. These previous studies provide comprehensive understandings of the AFHTL in a magnetic field and serve as reasonable benchmarks for the quantum phase diagram.

Below, we present our investigation of the AFHTL using DMMFT. For benchmarking purposes, we also performed a calculation with the state-of-the-art technique DMRG. We compare our results obtained with DMMFT to those from DMRG as well as results reported in the literatures. Remarkably, we find quantitative agreement between the results obtained with DMMFT and those from the more sophisticated methods. This alignment is achieved with a small cluster of just three lattice sites in DMMFT, demonstrating the efficiency of the method.

The Hamiltonian describing the AFHTL in a longitudinal external field includes both the exchange interactions and the Zeeman couplings,

$$H_{\text{AFH,Z}} = H_{\text{AFH}} + H_Z, \quad (22)$$

where $H_Z = -\sum_i g\mu_B h_z S_i^z$. In our DMMFT calculations, we set the gyromagnetic factor $g\mu_B = 1$ and h_z is measured in the corresponding natural unit.

Four phases emerge in the AFHTL with generic easy-axis anisotropy under a longitudinal external magnetic field. They are the coplanar “Y”-shaped phase, the collinear up-up-down (UUD) phase, the coplanar “V”-shaped phase, and the collinear polarized phase, in the order of increasing h_z . All these phases are compatible with a cluster partition of three lattice sites and translational symmetries. A simple order parameter distinguishing these phases is the magnetization along the easy axis, i.e.,

$$M_c^z = \sum_{i \in c} S_i^z = S_A^z + S_B^z + S_C^z, \quad (23)$$

where the subscript $i = A, B, C$ labels three sublattice sites within the cluster c . The polarized and the UUD phases are characterized by magnetization plateaux at $M_c^z = M_{c,(s)}^z$ and $M_c^z = M_{c,(s)}^z/3$, respectively, where $M_{c,(s)}^z = \frac{3}{2}$ is the saturation magnetization of the cluster. The “V”-shaped phase is sandwiched in between the UUD and the polarized phases, while the “Y”-shaped phase appears at low fields. A distinguishing order parameter characterizing the non-collinearity of the “Y”-shaped phase is the vector chirality

$$\boldsymbol{\kappa}_V = \frac{8}{3\sqrt{3}} (\mathbf{S}_A \times \mathbf{S}_B + \mathbf{S}_B \times \mathbf{S}_C + \mathbf{S}_C \times \mathbf{S}_A), \quad (24)$$

where the normalization factor is chosen such that $|\boldsymbol{\kappa}_V| = 1$ for the 120° -Néel state of $S = \frac{1}{2}$ spins without being renormalized by quantum fluctuations.

Despite that all four phases are homologous to their corresponding semiclassical Néel ordered states, the quantum fluctuations play crucial roles in the “Y”-shaped and UUD phases. Specifically, quantum fluctuations lift the accidental degeneracies in the semiclassical ground state manifold, which is known as quantum order-by-disorder [56, 57], and significantly renormalize the magnitudes of the ordered spins [44–46] as well as the order parameters.

¹We thank the anonymous referee for pointing Refs. 47–50 to us. Cf. Ref. 50 and references therein for earlier studies.

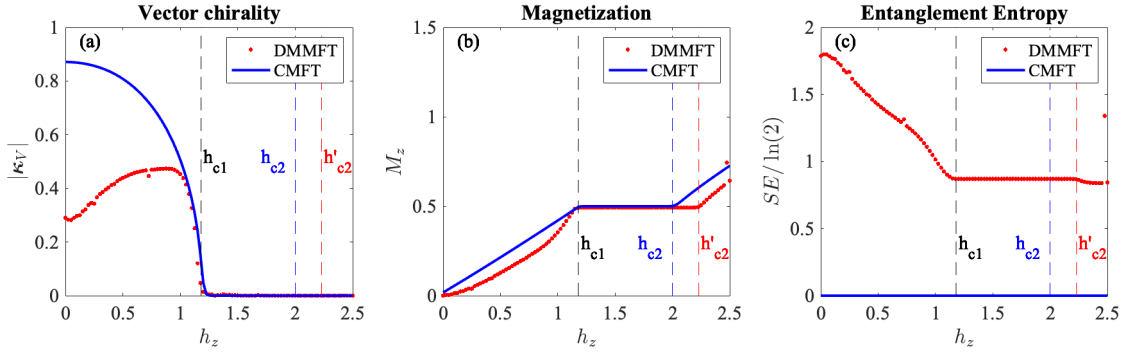


Figure 2: Phase diagram of AFHTL in a longitudinal magnetic field ($\mathcal{A} = 0.9$). (a) Vector chirality. (b) Magnetization. (c) Entanglement Entropy. Red dots represent DMMFT results, while blue curves depict conventional mean-field theory (CMFT) results. Vertical dashed lines indicate phase boundaries. h_{c1} distinguishes the “Y”-shaped phase from the UUD phase, where DMMFT and CMFT are in agreement. h_{c2} distinguishes the UUD-shaped phase from the “V”-shaped phase. Determined from the magnetization curves, the value of h_{c2} in blue from CMFT exhibits a discernible difference compared to h'_{c2} in red from DMMFT.

In our DMMFT calculations, we choose an extended cluster \bar{c} comprising of four three-lattice clusters with periodic boundary conditions. Employing the periodic boundary conditions is to minimize the boundary effects, since the Hilbert subspaces selected by the reduced DM is sensitive to the boundary conditions as known in DMRG [70]. The geometry and implementation details of DMMFT for the AFHTL are elaborated in Append. B, along with provided pseudocodes.

In Fig. 2, we present the dependence of the vector chirality, the magnetization, and the entanglement entropy of the ground states of AFHTL (with anisotropy parameter $\mathcal{A} = 0.9$) on the longitudinal magnetic field, calculated with the DMMFT (red) and the conventional MFT (blue). The cut-off parameter n_c , as discussed in Sec. 2.3 interpolating the conventional MFT and the DMMFT, is set to $n_c = 4$ for the DMMFT and $n_c = 1$ for the conventional MFT.

In Fig. 2(a), the vector chirality calculated with conventional MFT decreases monotonically as h_z increases in the “Y”-shaped phase and vanishes in the UUD and the “V”-shaped phases. In sharp contrast, the vector chirality calculated with DMMFT, does not decrease monotonically in the “Y”-shaped phase. Notably, the vector chirality at $h_z = 0$ in DMMFT is only about 30% of that in conventional MFT. The discrepancy reflects the renormalization of the ordered spins due to the quantum fluctuations. Upon closer examination of the magnitude of the ordered spins, for a small anisotropy $\mathcal{A} = 0.9$, we find $|\langle S \rangle| = 0.269 \pm 0.014$. This value, only about 50% of $S = \frac{1}{2}$, aligns with expectations based on previously reported values [44–46]. Given that κ_V scales as S^2 , a reduction factor of approximately 25% is expected for the magnitude of the vector chirality at $h_z = 0$. The curves of the DMMFT and the conventional MFT converge as h_z increases, both vanishing beyond h_{c1} (the critical field separating the “Y”-shaped and the UUD phases determined according to the magnetization curves). With stronger h_z , the spins are aligned closer to the easy axis, and the effect of the quantum fluctuations weakens, which is clearly evidenced from the monotonically decreasing entanglement entropy in the “Y”-shaped phase as shown in Fig. 2(c). Therefore, the suppression of the quantum fluctuations and the alignment of the spins towards the collinear UUD configuration by the longitudinal magnetic field jointly lead to the non-monotonic dependence of the vector chirality $|\kappa_V|$ on h_z .

In Fig. 2 (b), notable differences are apparent in the magnetization curves as predicted by DMMFT and conventional MFT. Particularly, DMMFT exhibits a nonlinear magnetization

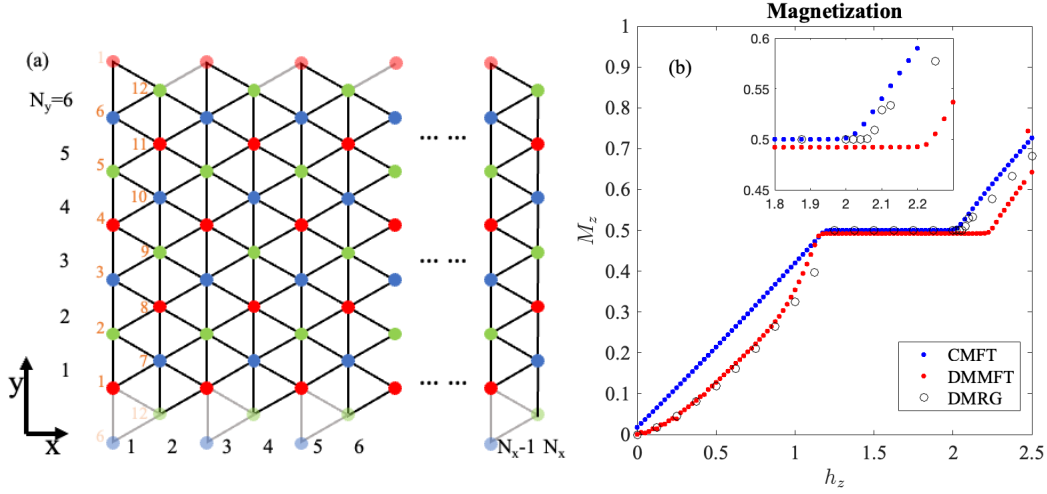


Figure 3: (a) Cylindrical geometry YCN_y-N_x of a triangular lattice for DMRG calculations. Translucent sites and bonds represent the extended triangular lattice under the periodic boundary condition. Sites in the tensor string are labelled by numbers in orange. (b) Magnetization curve of the AFHTL in longitudinal magnetic field ($\mathcal{A} = 0.9$). The results of CMFT (blue dots), DMMFT (red dots), and DMRG (black circles) are overlaid. The inset provides a zoomed-in view around the transition between the UUD phase and the “V”-shaped phase.

curve at low fields in the “Y”-shaped phase and a wider plateau supporting the UUD phase. To benchmark our results, we also perform a calculation of the magnetization using the state-of-the-art technique DMRG [71]. We consider a triangular lattice with $N_x \times N_y$ sites as shown in Fig. 3(a). We impose the periodic boundary condition along y -direction, or equivalently wrap the triangular lattice on a cylinder with its axis parallel to the x -direction. (The translucent sites and bonds represent the extended triangular lattice under the periodic boundary condition to guide visualization.) Since one edge of the triangular lattice is parallel to the y -direction, we refer to this geometry as YCN_y-N_x , following the convention used in the literatures [61, 62, 65, 66], where N_y is the circumference and N_x is the length of the cylinder. A tensor string winds through the system helically as $i_s = N_y(n_x - 1) + n_y$, where i_s labels the site in the tensor string [shown as orange numbers in Fig. 3(a)], and n_x and n_y are integer coordinates of the sites in the x - and y -directions.

Fig. 3(b) shows the magnetization curve calculated with DMRG for YCN_6-30 and bond dimension $D_b = 400$ (black circles), overlaid with the results of conventional MFT (blue dots) and DMMFT (red dots). The DMRG results are in excellent agreement with the DMMFT results, confirming the nonlinear magnetization in low field. Additionally, a self-consistency check for the choice of $n_c = 4$ in DMMFT can be confirmed from the entanglement entropy in the “Y”-shaped phase. At $h_z = 0$, we have $SE_c \approx 1.8 \ln(2)$. Therefore, $\tilde{D}_c^E = [\exp(SE_c)] = 4$.

On the other hand, as h_z surpasses h_{c2} , the system transitions towards the “V”-shaped phase, deviating from the $\frac{1}{3}$ magnetization plateau of the UUD phase. Fig. 2(b) demonstrates a discernible difference in the critical field determined from the magnetization curves in DMMFT ($h'_{c2} \approx 2.2$) and in conventional MFT ($h_{c2} \approx 2.0$). Notably, the range of the field stabilizing the UUD phase in DMMFT is larger than that in conventional MFT. Although the UUD configuration is homologous to its semiclassical correspondence, quantum fluctuations contribute significantly to stabilize the UUD phase [52]. Especially in the Heisenberg limit, the UUD phase is stable only $h_z = h_{c2} = \frac{1}{3}h_z^{(s)} = 1.5$ ($h_z^{(s)}$ is the saturation field) in the classical phase

diagram, whereas it extends to a finite field range due to quantum fluctuations in the quantum phase diagram. A similar effect of quantum fluctuations is also anticipated when $\mathcal{A} < 1$. Since n_c used in DMMFT is larger than that in conventional MFT, which includes more quantum fluctuations, a larger field range ($h'_{c2} > h_{c2}$) that stabilizes the UUD phase is expected.

To provide a quantitative comparison, we further compare the value of h_{c2} obtained from DMMFT to those estimated from our DMRG results and those inferred from the literatures. The inset of Fig. 3(b) provides a zoomed-in view of the transition between the UUD phase and the “V”-shaped phase. Our DMRG results indicate $h_{c2}^* \approx 2.06$, which falls between the h_{c2} of conventional MFT and h'_{c2} of DMMFT. Few precise values of h_{c2} for $\mathcal{A} = 0.9$ have been reported in the literatures [47–49, 52, 53]. Inferring from the reported values of h_{c2} for the isotropic Heisenberg model, we conclude that the h_{c2}^* estimated from our DMRG results may have slightly underestimated the critical field, probably due to the finite-size effect of $N_y = 6$ along the transverse direction of the cylinder [compared to Fig. 1 in Ref. 48 and Fig. 7(a) in Ref. 53 for scaling to thermodynamic limit]. Whereas h'_{c2} estimated from our DMMFT results may have slightly overestimated the critical field due to our choice of $n_c = 4$, which is larger than the speculated optimal $n_c^* = 2$ estimated from the entanglement entropy. This leads to an inclusion of too many quantum fluctuations favoring the UUD phase. Moreover, as h_z drives the system deeper inside the “V”-shaped phase, the magnetization curve obtained from our DMRG calculation gradually converges towards that of DMMFT.

In conclusion, our study of the AFHTL highlights the systematic improvement made by DMMFT over the conventional MFT. Remarkably, even with just a small cluster of three lattice sites, DMMFT achieves precision comparable to that of large system sizes calculated using DMRG or conventional MFT plus scaling. This underscores the efficiency and efficacy of DMMFT in capturing the effects of quantum fluctuations.

4 Discussions

In Sec. 4.1, we undertake a comparative analysis of DMMFT with DMRG, DMFT, CVM, and LCE. Additionally, in Sec. 4.2, we extend the DMMFT for systems at finite temperatures, and in Sec. 4.3, we extend the DMMFT for systems with disorders.

4.1 Comparisons with Alternative Methods

4.1.1 Comparison with Density-Matrix Renormalization Group

We first compare DMMFT with DMRG. The constructions of the effective Hamiltonian appear similar, where the reduced DM is employed to select Hilbert subspace significant with respect to the target state. The resemblance between the DMMFT and the infinite DMRG is most pronounced when the spatial dimension $d = 1$ as illustrated in the AKLT model in Sec. 3.1. The primary difference lies in where the Hilbert space $\tilde{\mathcal{H}} = \mathcal{H}_c \otimes \tilde{\mathcal{H}}_c$ is chosen. In DMMFT, the projector $\Pi_{c'}$ is iteratively optimized solely over the Hilbert space $\mathcal{H}_{c'}$ without changing the cluster size of the environment. Conversely, in infinite DMRG, the environment is constructed iteratively over the Hilbert space of the semi-infinite chains. Gauged by the quantum entanglement, the dimension of the Hilbert subspace selected for constructing the effective Hamiltonian is bounded by \tilde{D}_c^E [Eq. (16)] in both cases. As \tilde{D}_c^E is bounded by the size of the cluster c , DMRG can feasibly select a finite significant Hilbert subspace without being hindered by the infinite size of the environment asymptotically. On the contrary, in DMMFT, we assume that the significant Hilbert subspace resides within $\mathcal{H}_{c'}$, which is a reasonable approximation, especially for short-range entangled systems. Ignoring practical constraints provided we choose the cluster size being larger than the typical entanglement range, DMMFT and DMRG

are equivalent in $d = 1$.

The advantages of DMMFT become more significant in higher dimensions, $d \geq 2$. In DMRG, a d -dimensional system is compactified to a quasi-one-dimensional system, and an artificial one-dimensional string of clusters winds through the system as shown in Fig. 3(a). Consequently, even in the case of a short-range entangled system, artificial long-range entanglements emerge for sites physically close but distant along the string. The entanglement between physically neighboring clusters scales exponentially with N_{\perp}^{d-1} , where N_{\perp} represents the linear scale of the system along the transverse directions. In contrast, DMMFT makes use of the separability [Eq.(17)] enables the study of local problems over extended clusters without introducing artificial long-range entanglements arising from the transverse dimensions. From this perspective, DMMFT may be regarded as a mean-field approximation of DMRG and proves particularly valuable for short-range entangled systems in higher dimensions.

4.1.2 Comparison with Dynamical Mean-Field Theory

We proceed to compare DMMFT with DMFT. In DMFT, designed for fermionic systems, the effective action is constructed over a local cluster, employing the single-particle Green's function as a dynamical mean-field to capture the fluctuations [19, 20]. This local problem, entailing a dynamical mean-field, is subsequently mapped to an effective impurity model and solved using ED or QMC kernels [19]. In contrast to the Anderson impurity model tailored for fermions, devising an equivalent impurity model for spins is not straightforward. Furthermore, even if a spin impurity model consistent with the principles of DMFT could be formulated, the challenge of efficiently solving it would remain. Constructing a generic spin impurity (if not impossible) can introduce significant frustrations, which leads to the failure of the QMC kernel due to the sign problem. On the other hand, achieving an accurate representation of the environment requires incorporating a large number of spins beyond those in the local cluster, which causes the ED kernel to rapidly encounter the exponential wall. A simplification of DMFT proposed in DMET for fermionic systems involves utilizing the local density matrix, a static observable, instead of the dynamical Green's function [21]. While a formal generalization of DMET to spin systems is feasible, the challenge lies in identifying a suitable reference wave-function that facilitates straightforward Schmidt decomposition and the construction of the embedding Hamiltonian. On the contrary, in DMMFT, the reduced DM is generally defined for many-body states, making DMMFT naturally applicable to fermions, bosons, as well as spins.

An alternative approach to investigating the ground state of a quantum many-body system is to work directly with the wave function. One example can be the Gutzwiller method, which uses Gutzwiller wave-function as an variational Ansatz [72–75]. The Gutzwiller approximation can be viewed as a quantum embedding approach in a unified perspective with DMFT and DMET [76]. More recently, VDAT has been proposed to solve the shortcomings of Gutzwiller Approximation and simplify the computational complexity of DMFT. In VDAT, the variational ansatz is the sequential product density matrix, which is evaluated via the discrete action theory [22, 23]. The VDAT Ansatz is controlled by an integral parameter \mathcal{N} , and it is asymptotically exact as \mathcal{N} tends to infinity but also becomes more computationally demanding. While it has been demonstrated that VDAT can yield accurate ground state wave functions for fermionic systems, even with \mathcal{N} as small as 3 [24, 25], it faces challenges when applied to spin systems. Constructing the sequential product density matrix for the spin system is straightforward; however, the absence of Wick's theorem for spin systems presents a challenge in efficiently applying discrete action theory to evaluate the Ansatz.

Moreover, integrating wave function approaches with DMMFT raises the question of determining a global state from reduced density matrices of local clusters. This challenge is recognized as the quantum marginal problem [77]. Finding a general solution to this problem is currently beyond the scope of this paper and remains an open and challenging research

question [78].

It deserves particular comments on the lattice symmetries when comparing DMMFT with cluster extensions of DMFT. The problem of the lattice symmetry is a shared problem not only for DMFT but also for all cluster approaches formulated in real space. In cluster extensions of DMFT, this challenge arises because the approximate self-energy might not preserve the underlying lattice symmetry. Inconsistencies may arise if artificial periodization is not appropriately imposed [79]. In contrast, DMMFT works with local static Hamiltonians, which allows for a more straightforward imposition of symmetrization. Let $G = g$ denote a subgroup of symmetry transformations of the lattice that one would enforce, and denote the representations of g over \mathcal{H} as \tilde{g} . Then, the mean-field Hamiltonian in Eq. (11) can be symmetrized as

$$\tilde{H}_{\text{MF,Symm}}^{(c)} = \frac{1}{|G|} \sum_{g \in G} \tilde{g} \tilde{H}_{\text{MF}}^{(c)} \tilde{g}^{-1}. \quad (25)$$

Given that the reduced density matrix is constructed from the eigenstates of the Hamiltonian, it should naturally respect the corresponding symmetries inherited from the symmetrized Hamiltonian $\tilde{H}_{\text{MF,Symm}}^{(c)}$.

4.1.3 Comparison with Cluster Variation Method

CVM is a variational method minimizing the free energy

$$F[\rho] = \text{Tr}(\rho H) + k_B T \text{Tr}[\rho \ln(\rho)], \quad (26)$$

with respect to the density matrix. In Eq. (26), ρ is the many-body DM for the entire system, k_B is the Boltzmann constant, and T is the temperature. For Hamiltonian consisting of terms with finite-range interactions, it is sufficient to know up to n -point reduced DM,

$$\rho^{(n)}(\{i_1, i_2, \dots, i_n\}) = \text{Tr}_{\mathcal{I} \setminus \{i_1, i_2, \dots, i_n\}} \rho, \quad (27)$$

for evaluating the energetic contribution $\text{Tr}(\rho H)$ to the free energy, where the set $\{i_1, i_2, \dots, i_n\}$ supports of the terms in the Hamiltonian. For example, in Heisenberg models with exchange interactions and Zeeman couplings, it only requires $\rho^{(n=2)}(i_1, i_2)$ where the distance $|i_1 - i_2|$ is bounded by the interaction range of the Hamiltonian. The key idea of the CVM is to use cluster entropies for evaluating the entropic contribution $\text{Tr}[\rho \ln(\rho)]$ to the free energy. The cluster entropies rely only on the reduced DMs supporting the clusters and are expected to decay rapidly when the linear size of the clusters exceeds the correlation length of the system [32]. The cluster approximation involves selecting a truncation in cluster size. A particular choice of the truncation for models with Heisenberg exchange interactions is at second order, i.e., $n = 2$, which is also known as the pair approximation [29–31]. In this approach, the variational equations, along with the consistency conditions of the reduced DM, lead to the effective mean-field Hamiltonians of conventional MFTs [30, 31] and the separability $\rho^{(n=2)}(i, j) = \rho^{(n=1)}(i) \otimes \rho^{(n=1)}(j)$ for $|i - j|$ exceeds the interaction range [29].

The separability in CVM arises as a consequence of the absence of long-range interactions and the truncation at $n = 2$. However, quantum fluctuations can manifest as entanglements over longer range, which is inherently determined by the nature of quantum states. In this sense, DMMFT improves over CVM with pair approximation by considering the quantum entanglements over the range of the extended cluster and determining the reduced DM ρ_c self-consistently, up to $n = |c|$.

Another question worth mentioning is whether the mean-field equations derived in Sec. 2 can be derived from the perspective of CVM. As demonstrated in Ref. 29, conventional mean-field theories [30, 31] can be derived as special cases of CVM with pair approximation and

constant-coupling approximation. Different choices of consistency conditions can lead to different conventional mean-field theories [30, 31]. In this article, we have derived the mean-field equations for DMMFT by assuming the separability for distant clusters. However, whether separability can emerge as a natural consequence of alternative approximations beyond pair approximation, as demonstrated for conventional MFTs in CVM in Ref. 29), remains an open question. We do not have an answer to this question and leave it for future research.

4.1.4 Comparison with Linked-Cluster Expansion

LCE is another cluster-based method used for analyzing quantum spin systems [33–37, 39, 40]. Beyond conventional MFTs, the corrections from quantum and thermal fluctuations are represented in terms of a series of x^n , where $x = H_I/(k_B T)$ and H_I is part of the Hamiltonian describing the fluctuations [33–35]. Considering the series as a perturbative expansion ordered by the power n , x can surpass the radius of convergence of the series at sufficiently low temperatures, which poses a challenge for convergence in LCE. This obstacle is better overcome by numerical LCE, where physical observables are calculated still in a basis as in LCE but not perturbatively in temperature [36, 37]. Then, it is the correlation length, instead of the temperature, that determines the convergence of the series. Consequently, numerical LCE can converge at a lower temperature than perturbative LCE. However, if long-range order develops at low temperature, and the correlation length becomes larger than the cut-off scale of the cluster sizes, the convergence is no longer guaranteed [38]. Resummation algorithms, such as Wynn’s algorithm, Brezinski’s algorithm [80], and Euler’s transformation [81], have been developed to accelerate the convergence of numerical LCE [38].

In DMMFT, the cluster partition is fixed at the beginning, and there are no summations over various configurations of the clusters. Although the size of the clusters plays a similar role in DMMFT and numerical LCE, setting the cut-off scale for the correlated fluctuations, DMMFT does not suffer from convergence problems even if long-range order develops at low temperatures because there are no explicit summations needed. Moreover, for practical applications, numerical LCE needs to handle a large number of large clusters of various sizes (often solved by ED), which can be computationally demanding. In this regard, DMMFT can outperform LCE in computational efficiency particularly at low temperatures.

4.2 Systems at Finite Temperatures

The extension of DMMFT for systems at finite temperatures is straightforward. In Eq.(9), we use the ground state of the effective Hamiltonian over the extended cluster to compute the reduced DM. At finite temperatures, assuming local thermal equilibrium, we can average the reduced DMs of the eigenstates weighted by the Boltzmann distribution. Specifically, let $\{E_\alpha, |\tilde{\phi}_\alpha\rangle\}$ be the eigensystems of $\tilde{H}_{\text{MF}}^{(c)}$. Then, the thermally averaged reduced DM is given by

$$\begin{aligned} [\rho_c^{\text{MF}}]_T &= \sum_{\alpha} w_{\alpha} \rho_c^{\alpha}, \\ w_{\alpha} &= \frac{\exp[-E_{\alpha}/(k_B T)]}{\sum_{\beta} \exp[-E_{\beta}/(k_B T)]}, \\ \rho_c^{\alpha} &= \text{Tr}_{\tilde{c}} |\tilde{\phi}_{\alpha}\rangle \langle \tilde{\phi}_{\alpha}|, \end{aligned} \quad (28)$$

where the square bracket with a subscript T indicates the thermal average. As discussed in Sec. 2.3, when $D_{\mathcal{H}_{c'}} = 1$, DMMFT reduces to the CMFTs at zero temperature. It is straightforward to check that, since $[\rho_c^{\text{MF}}]_T \sim \exp[-\tilde{H}_{\text{MF}}^{(c)}/(k_B T)]$ when $D_{\mathcal{H}_{c'}} = 1$, the extension of DMMFT according Eq.(28) also aligns with the conventional MFTs at finite temperatures.

However, it is worth noting that the thermal averaging in Eq.(28) does not fully capture all thermal fluctuations. Specifically, at low temperatures, it is often the gapless long wave length modes (Goldstone modes) that dominate the thermal fluctuations. However, due to the mean-field approximation inherent in DMMFT, these thermal fluctuations are frozen by the assumption of translational symmetry. Therefore, similar to all other mean-field methods, DMMFT tends to underestimate the impact of thermal fluctuations at finite temperatures.

4.3 Systems with Disorders

Disorders are an inevitable aspect of experiments. Even minuscule amounts of disorders can alter the nature of fragile quantum phases, particularly in the frustrated systems. Consequently, it becomes crucial to incorporate disorders into the DMMFT framework.

In the presence of the disorders, the Hamiltonian of the extended cluster undergoes direct modification, denoted as

$$H[\mathcal{O}_{\bar{c}}] \rightarrow H^{(\delta)}[\mathcal{O}_{\bar{c}}], \quad (29)$$

where the superscript δ labels the types of the disorders. However, the process of averaging over disorders is more intricate than the thermal average discussed in Sec. 4.2.

Consider a straightforward scenario involving a single magnetic vacancy in the cluster c , wherein there can be either no vacancies or one vacancy on a site $i \in c$. In this case, we denote $\delta \in \Delta = \{0\} \cup c$, where $\delta = 0$ signifies no vacancies in the cluster c . We assume the probability measure of the disorder configurations to be $P_{\Delta}(\delta)d\delta$. Analogous to Eq.(28), it is intuitive to define an average over the disorders as

$$[\rho_c^{\text{MF}}]_{\Delta, \text{ann}} = \int_{\Delta} \rho_c^{(\delta)} P_{\Delta}(\delta) d\delta, \quad (30)$$

$$\rho_c^{(\delta)} = \text{Tr}_{\bar{c}} |\tilde{\phi}_{(\delta)}\rangle \langle \tilde{\phi}_{(\delta)}|,$$

where $\tilde{\phi}_{(\delta)}$ is the ground state of the effective Hamiltonian $\tilde{H}_{\text{MF}}^{(c),(\delta)}$, and the square bracket with a subscript Δ indicates the average over the disorder configurations. The physical meaning of $[\rho_c^{\text{MF}}]_{\Delta, \text{ann}}$ so-defined requires further clarification. When $[\rho_c^{\text{MF}}]_{\Delta, \text{ann}}$ is employed to set the effective environment $\mathcal{C}'_c = \{c'\}$ for the cluster c , each c' is already averaged over various disorder configurations according to Eq.(30). In other words, the disorders are *annealed*. For this reason, we also add the subscript “ann” in Eq.(30).

In experiments, magnetic vacancies often exhibit behavior more akin to static disorders than fluctuating disorders, particularly when the vacancies are not thermally migrating. Disorders as such are often referred to as *quenched* disorders, in contrast to the annealed disorders. In this case, we consider all possible disorder configurations over the extended cluster \bar{c} . Assume \bar{c} consisting of ν simple clusters, including the focused cluster c and $\nu - 1$ clusters in the environment. If the simple clusters are identical, all possible disorder configurations of the quenched disorders form a set $\mathbf{\Delta} = \Delta^{\nu} = (\delta_1, \delta_2, \dots, \delta_{\nu})$. We obtain coupled mean-field equations for $\{\rho_c^{(\delta)}\}_{\mathbf{\Delta}}$. Once $\{\rho_c^{(\delta)}\}_{\mathbf{\Delta}}$ is solved, the expectation values of local observables averaged over the quenched disorders should be calculated as

$$[\langle O_i^{\alpha} \rangle]_{\Delta, \text{quen}} = \int_{\mathbf{\Delta}} \text{Tr}_c [O_i^{\alpha} \rho_c^{(\delta)}] P_{\mathbf{\Delta}}(\delta) (d^{\nu} \delta), \quad (31)$$

where $P_{\mathbf{\Delta}}(\delta)(d^{\nu} \delta)$ is the probability measure over the configuration space of the quenched disorders $\mathbf{\Delta}$. In the special case where each vacancy is independent and subjected to an identical distribution $P_{\Delta}(\delta)d\delta$, then $P_{\mathbf{\Delta}}(\delta)(d^{\nu} \delta) = \prod_{n=1}^{\nu} P_{\Delta}(\delta_n)d\delta_n$.

In real systems, the effects of disorders can be more complicated. For instance, there can be cluster of vacancies due to lower formation free energy, and the probability measure of the vacancies no longer takes the simple product form. Moreover, disorders can manifest as inhomogeneity of the samples, especially when scale of the probe is small, and the effects of disorders are not self-averaged in the experiments. Despite of the complications of disorders arising in real systems, DMMFT can, in principle, be adapted to include the disorder effects accordingly.

5 Conclusion

In this study, we introduce a novel mean-field approach, DMMFT, specifically designed to capture quantum fluctuations beyond conventional MFTs. Combining the strengths of DMRG and DMFT, DMMFT stands out as an efficient and unbiased method applicable to fermions, bosons, and spins, even in the presence of frustrations. A notable feature of DMMFT is its capability to discern topological phases enabled by its utilization of the reduced DM, as demonstrated with the example of the AKLT model in Sec. 3.1. Furthermore, DMMFT can achieve precision comparable to DMRG, even with only a small cluster, as demonstrated with the example of the AFHTL in Sec. 3.2. Additionally, DMMFT seamlessly extends to systems at finite temperatures and with disorders. In conclusion, DMMFT provides an effective tool for exploring phases exhibiting unconventional quantum orders. It can be particularly beneficial for investigating frustrated spin systems in high spatial dimensions.

Acknowledgements

This work is supported as part of the Institute for Quantum Matter, an Energy Frontier Research Center funded by the U.S. Department of Energy, Office of Science, Office of Basic Energy Sciences, under Award DESC0019331. This work is also partially supported by the NSF CAREER Grant DMR-1848349. JYZ is additionally supported by TIPAC from the Department of Physics and Astronomy, Johns Hopkins University. ZC is supported by the Columbia Center for Computational Electrochemistry. JYZ acknowledges motivating discussions with Collin Broholm, Oleg Tchernyshyov, and Tong Chen. JYZ also thanks Salvia Felixsen Skogen for the hospitality at Domini Katzen Institute.

A Iterative Algorithm for Mean-Field Equations

In Section 2.2, we established a closed set of coupled mean-field equations for DMMFT, delineated by Eqs. (9) to (14). Here, we present an iterative algorithm, as outlined in Table 1, to achieve self-consistent solutions numerically.

There remain some noteworthy considerations. In Step 0, while a stable self-consistent solution should be independent of initial values, providing an initial guess close to the self-consistent solution often aids convergence. An empirical approach is to start with a trivial ρ_c that can be constructed from solutions of conventional MFTs. In Step 0', a linear interpolation of the reduced DM

$$\rho_c^{(n+1)} = (1 - \alpha)\rho_c^{(n)} + \alpha\rho_c^{(n,\text{new})}, \quad (32)$$

can be employed for updating ρ_c . Here, $\rho_c^{(n)}$ represents the reduced DM used in Step 0 at the n -th iteration, and $\rho_c^{(n,\text{new})}$ is the new reduced DM obtained in Step 0', The learning rate α

Step number	Step description
0	Initialize a set of trial reduced DMs $\{\rho_c\}_{c \in \mathcal{C}}$.
For each cluster c :	
1	Diagonalize ρ_c , and construct Π_c according to Eq.(13).
2	Use Eq.(14) to construct $\Pi_{c'}$.
3	Use Eq.(10) to construct Π .
4	Use Eq.(11) to construct $\tilde{H}_{\text{MF}}^{(c)}$.
5	Diagonalize $\tilde{H}_{\text{MF}}^{(c)}$ and select the target state $ \tilde{\phi}_c\rangle$.
6	Calculate new ρ_c according to Eq.(9).
0'	Use new $\{\rho_c\}_{c \in \mathcal{C}}$ to update the trial reduced DMs, and repeat steps 1 - 6 until convergence.

Table 1: DMMFT implementation steps.

varies in the range $(0, 1)$. Larger values of α lead to a more rapid update, while smaller values contribute to stabilizing the iterative process.

Finally, the hyperparameter n_c used in Eq.(13) in Step 1 can be compared to $\tilde{D}_c^E = \lceil \exp(SE_c) \rceil$, where the entanglement entropy is calculated according to Eq.(8). It is important to note that setting $n_c = 1$ should recover the results of conventional MFTs.

B Pseudocodes for Heisenberg Model

In this Appendix section, we describe the implementation of DMMFT for the AFHTL that has been discussed in Sec. 3.2.

We choose a cluster partition of the triangular lattice with each cluster comprising three lattice sites as shown in Fig. 4. The hexagons represent the Wigner-Seitz cells of the three-lattice clusters compatible with the symmetries of the underlying triangular lattice. The central cluster c is highlighted in orange. We choose an extended cluster \bar{c} comprising of four three-lattice clusters $\{c; c'_1, c'_2, c'_3\}$ with periodic boundary conditions. Fig. 4 shows the extended cluster in a periodically extended scheme, i.e., clusters in \mathcal{C}'_c have been duplicated under periodic translations \mathbf{a}_i . Bonds depicted in solid lines indicate intra-cluster couplings contained in H_c , while dashed lines indicate inter-cluster couplings contained in H_{c, c'_i} . For visual clarity, Fig. 4 has abbreviated some coupling bonds.

Now, we proceed to describe the pseudocodes of DMMFT.

First, we define the local degrees of freedom. For the AFHTL, on each site, there is a quantum spin of $S = \frac{1}{2}$. We define $S_i^\alpha, \alpha = x, y, z$ and the identity operator for each site as follows.

```

1 '# Code Block 1: define the physical site: S=1/2 #'
2 % length of the spin
3 slen = 1.0/2.0;
4 % dimension of local Hilbert space
5 dimHi = 2;
6 % define local operators
7 idiop = eye(dimHi);
8 sxop = [0.0, 1.0; 1.0, 0.0]*slen;
9 syop = [0.0, -1.0j; 1.0j, 0.0]*slen;
10 szop = [1.0, 0.0; 0.0, -1.0]*slen;

```

Next, we define the local operators for the clusters shown in Fig. 4. These local operators for cluster c are constructed from the site operators by tensor product, which are then

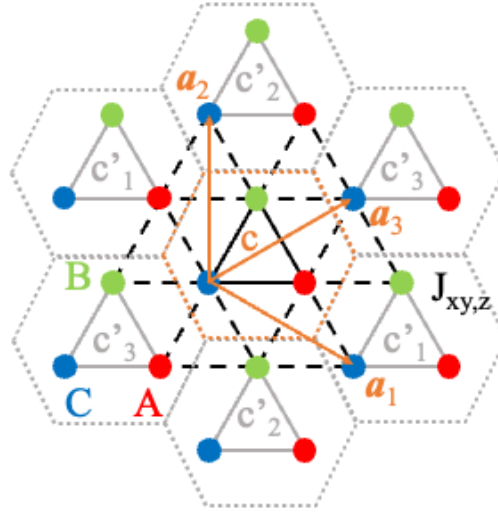


Figure 4: Extended cluster with periodic boundary conditions. The hexagons represent the Wigner-Seitz cells of the three-lattice clusters compatible with the symmetries of the underlying triangular lattice. The central cluster c is highlighted in orange. Three neighboring clusters in $\mathcal{C}'_c = \{c'_1, c'_2, c'_3\}$ have been duplicated under periodic translations a_i . Bonds depicted with solid lines indicate intra-cluster couplings contained in H_c , while dashed lines indicate inter-cluster couplings contained in H_{c,c'_i} . For visual clarity, not all coupling bonds are shown.

represented in matrix form using the `kron()` function.

```

1 '# Code Block 2: define local operators for cluster c #'
2 % number of sites in c
3 nsite = 3;
4 % dimension of the cluster Hilbert space
5 dimHc = dimHi^nsite;
6
7 idcop = eye(dimHc);
8 opclist = {idcop};
9
10 for isite in c:
11     % construct siaop as tensor products of idiop's saop
12     % for example: slxop = kron(sxop, kron(idiop, idiop))
13     opclist.append(siaop);
14 end for % isite

```

With local operators, the Hamiltonian H_c containing intra-cluster exchange interactions and Zeeman couplings is constructed according to their definitions as follows.

```

1 '# Code Block 3: construct Hamiltonian of intracluster couplings #'
2 Hamc = zeros(dimHc);
3 % add exchange interactions
4 for ibond in c:
5     i, j = vertex(ibond);
6     Hamc = Hamc + sum_a Ja*siaop*sjaop;
7 end for % ibond
8 % add Zeeman couplings
9 for isite in c:
10     Hamc = Hamc - sum_a ha*siaop;
11 end for % isite

```

Then, we define the operators for the extended cluster \bar{c} .

```

1 '# Code Block 4: define operators for the extended cluster cbar #'
2 % number of clusters in cbar
3 ncbars = 4;
4 % dimension of the cluster Hilbert space
5 dimHcbar = dimHc*dimHcp^(ncbars-1); % cf. Eq.(10)
6
7 idcbarsop = eye(dimHcbar);
8 opcbarslist = {idcbarsop};
9
10 % construct spin operators
11 for isite in cbar:
12     % construct siabarsop as tensor products of idcop's siaop
13     % for example: sixbarsop = kron(sixop,kron(idcop,kron(idcop,idcop)))
14     opcbarslist.append(siabarsop);
15 end for % isite
16
17 % construct Hamiltonian operator with intra- and inter-cluster terms
18 Hamcbar = sum_c Hamc + sum_{c,cp} Hamccp;

```

Finally, we solve the mean-field equations self-consistently. We use the iterative method solving the mean-field equations, following the steps described in Append. A.

```

1 '# Code Block 5: Iterative solver #'
2 '> step 0: initialization <'
3 rhoc = reduced DM from classical spin configurations
4
5 % configure iteration process
6 % learning rate
7 alearn = 0.6;
8 % cut-off dimension, n_c
9 dimHcp = 4;
10
11 % start iterations
12 while (not converge):
13     '> step 1: construct Projc [Eq.(13)] <'
14     evec_rhoc, eval_rhoc = eig(rhoc);
15     Projc = zeros(dimHc,nc);
16     for istate in largest n_c evals of rhoc:
17         Projc.append(evec_rhoc(istate));
18     end for % istate
19
20     '> step 2: construct ProjCp [Eq.(14)] <'
21     for ic in C':
22         ProjCp = kron(ProjCp,Projc)
23     end for % ic
24     '> step 3: construct Proj [Eq.(10)] <'
25     Proj = kron(idcop,ProjCp);
26
27     '> step 4: construct effective Hamiltonian [Eq.(11)] <'
28     Ham_MFeff = Proj'*Hamcbar*Proj;
29
30     '> step 5: find ground state of Ham_MFeff <'
31     evec_Ham, eval_Ham = eig(Ham_MFeff);
32     phicbar = state in evec_Ham with lowest energy;
33     rhocbar = phicbar*phicbar';
34
35     '> step 6: calculate new rhoc [Eq.(9)] <'
36     rhoc_new = partially tracing rhocbar over {c'};
37
38     '> step 0: update rhoc [Eq.(29)] <'
39     rhoc = (1-alearn)*rhoc + alearn*rhoc_new;

```

```
40 check convergence;  
41  
42 end while % iteration
```

The pseudocode provided above serves only to demonstrate how to implement DMMFT step-by-step. Considering the memory and time efficiencies, many optimizations can be employed. For example, one may use the Lanczos algorithm in Code Block 5, line 14 and line 31, since not the full spectra of ρ_c and $\tilde{H}_{\text{MF}}^{(c)}$ are used.

Funding information JYZ is supported by IQM EFRC DOE under Award DESC0019331, NSF CAREER under Grant DMR-1848349, and TIPAC PHA JHU. ZC is supported by the Columbia Center for Computational Electrochemistry.

References

- [1] L. Balents, *Spin liquids in frustrated magnets*, Nature **464**(7286), 199 (2010), doi:[10.1038/nature08917](https://doi.org/10.1038/nature08917).
- [2] M. J. P. Gingras and P. A. McClarty, *Quantum spin ice: a search for gapless quantum spin liquids in pyrochlore magnets*, Reports on Progress in Physics **77**(5), 056501 (2014), doi:[10.1088/0034-4885/77/5/056501](https://doi.org/10.1088/0034-4885/77/5/056501).
- [3] C. Broholm, R. J. Cava, S. A. Kivelson, D. G. Nocera, M. R. Norman and T. Senthil, *Quantum spin liquids*, Science **367**(6475), eaay0668 (2020), doi:[10.1126/science.aay0668](https://doi.org/10.1126/science.aay0668), <https://www.science.org/doi/pdf/10.1126/science.aay0668>.
- [4] P. W. Anderson, *Resonating valence bonds: A new kind of insulator?*, Mater. Res. Bull. **8**, 153 (1973), doi:[10.1016/0025-5408\(73\)90167-0](https://doi.org/10.1016/0025-5408(73)90167-0).
- [5] P. Fazekas and P. W. Anderson, *On the ground state properties of the anisotropic triangular antiferromagnet*, Philos. Mag. **30**, 423 (1974), doi:[10.1080/14786439808206568](https://doi.org/10.1080/14786439808206568).
- [6] V. Kalmeyer and R. B. Laughlin, *Equivalence of the resonating-valence-bond and fractional quantum Hall states*, Phys. Rev. Lett. **59**, 2095 (1987), doi:[10.1103/PhysRevLett.59.2095](https://doi.org/10.1103/PhysRevLett.59.2095).
- [7] A. Kitaev, *Anyons in an exactly solved model and beyond*, Annals of Physics **321**(1), 2 (2006), doi:<https://doi.org/10.1016/j.aop.2005.10.005>, January Special Issue.
- [8] C. Castelnovo, R. Moessner and S. L. Sondhi, *Magnetic monopoles in spin ice*, Nature **451**, 42 (2008), doi:[10.1038/nature06433](https://doi.org/10.1038/nature06433).
- [9] P. W. Anderson, *The resonating valence bond state in La_2CuO_4 and superconductivity*, Science **235**(4793), 1196 (1987), doi:[10.1126/science.235.4793.1196](https://doi.org/10.1126/science.235.4793.1196), <https://www.science.org/doi/pdf/10.1126/science.235.4793.1196>.
- [10] A. Kitaev, *Fault-tolerant quantum computation by anyons*, Annals of Physics **303**(1), 2 (2003), doi:[https://doi.org/10.1016/S0003-4916\(02\)00018-0](https://doi.org/10.1016/S0003-4916(02)00018-0).
- [11] S. R. White, *Density matrix formulation for quantum renormalization groups*, Phys. Rev. Lett. **69**, 2863 (1992), doi:[10.1103/PhysRevLett.69.2863](https://doi.org/10.1103/PhysRevLett.69.2863).
- [12] H. C. Jiang, Z. Y. Weng and D. N. Sheng, *Density matrix renormalization group numerical study of the kagome antiferromagnet*, Phys. Rev. Lett. **101**, 117203 (2008), doi:[10.1103/PhysRevLett.101.117203](https://doi.org/10.1103/PhysRevLett.101.117203).

- [13] S. Yan, D. A. Huse and S. R. White, *Spin-liquid ground state of the $S = 1/2$ kagome Heisenberg antiferromagnet*, *Science* **332**(6034), 1173 (2011), doi:[10.1126/science.1201080](https://doi.org/10.1126/science.1201080), <https://www.science.org/doi/pdf/10.1126/science.1201080>.
- [14] Z. Zhu, P. A. Maksimov, S. R. White and A. L. Chernyshev, *Topography of spin liquids on a triangular lattice*, *Phys. Rev. Lett.* **120**, 207203 (2018), doi:[10.1103/PhysRevLett.120.207203](https://doi.org/10.1103/PhysRevLett.120.207203).
- [15] G. Senatore and N. H. March, *Recent progress in the field of electron correlation*, *Rev. Mod. Phys.* **66**, 445 (1994), doi:[10.1103/RevModPhys.66.445](https://doi.org/10.1103/RevModPhys.66.445).
- [16] A. W. Sandvik, *Computational Studies of Quantum Spin Systems*, AIP Conference Proceedings **1297**(1), 135 (2010), doi:[10.1063/1.3518900](https://doi.org/10.1063/1.3518900), https://pubs.aip.org/aip/acp/article-pdf/1297/1/135/11407753/135_1_online.pdf.
- [17] P. W. Anderson, *Localized magnetic states in metals*, *Phys. Rev.* **124**, 41 (1961), doi:[10.1103/PhysRev.124.41](https://doi.org/10.1103/PhysRev.124.41).
- [18] J. Bardeen, L. N. Cooper and J. R. Schrieffer, *Theory of superconductivity*, *Phys. Rev.* **108**, 1175 (1957), doi:[10.1103/PhysRev.108.1175](https://doi.org/10.1103/PhysRev.108.1175).
- [19] A. Georges, G. Kotliar, W. Krauth and M. J. Rozenberg, *Dynamical mean-field theory of strongly correlated fermion systems and the limit of infinite dimensions*, *Rev. Mod. Phys.* **68**, 13 (1996), doi:[10.1103/RevModPhys.68.13](https://doi.org/10.1103/RevModPhys.68.13).
- [20] G. Kotliar, S. Y. Savrasov, K. Haule, V. S. Oudovenko, O. Parcollet and C. A. Marianetti, *Electronic structure calculations with dynamical mean-field theory*, *Rev. Mod. Phys.* **78**, 865 (2006), doi:[10.1103/RevModPhys.78.865](https://doi.org/10.1103/RevModPhys.78.865).
- [21] G. Knizia and G. K.-L. Chan, *Density matrix embedding: A simple alternative to dynamical mean-field theory*, *Phys. Rev. Lett.* **109**, 186404 (2012), doi:[10.1103/PhysRevLett.109.186404](https://doi.org/10.1103/PhysRevLett.109.186404).
- [22] Z. Cheng and C. A. Marianetti, *Variational discrete action theory*, *Phys. Rev. Lett.* **126**, 206402 (2021), doi:[10.1103/PhysRevLett.126.206402](https://doi.org/10.1103/PhysRevLett.126.206402).
- [23] Z. Cheng and C. A. Marianetti, *Foundations of variational discrete action theory*, *Phys. Rev. B* **103**, 195138 (2021), doi:[10.1103/PhysRevB.103.195138](https://doi.org/10.1103/PhysRevB.103.195138).
- [24] Z. Cheng and C. A. Marianetti, *Precise ground state of multiorbital mott systems via the variational discrete action theory*, *Phys. Rev. B* **106**, 205129 (2022), doi:[10.1103/PhysRevB.106.205129](https://doi.org/10.1103/PhysRevB.106.205129).
- [25] Z. Cheng and C. A. Marianetti, *Gauge constrained algorithm of variational discrete action theory at $\mathcal{N} = 3$ for the multiorbital hubbard model*, *Phys. Rev. B* **108**, 035127 (2023), doi:[10.1103/PhysRevB.108.035127](https://doi.org/10.1103/PhysRevB.108.035127).
- [26] T. Holstein and H. Primakoff, *Field dependence of the intrinsic domain magnetization of a ferromagnet*, *Phys. Rev.* **58**, 1098 (1940), doi:[10.1103/PhysRev.58.1098](https://doi.org/10.1103/PhysRev.58.1098).
- [27] D. P. Arovas and A. Auerbach, *Functional integral theories of low-dimensional quantum Heisenberg models*, *Phys. Rev. B* **38**, 316 (1988), doi:[10.1103/PhysRevB.38.316](https://doi.org/10.1103/PhysRevB.38.316).
- [28] R. Kikuchi, *A theory of cooperative phenomena*, *Phys. Rev.* **81**, 988 (1951), doi:[10.1103/PhysRev.81.988](https://doi.org/10.1103/PhysRev.81.988).

- [29] T. Morita and T. Tanaka, *Application of the cluster variation method to the Heisenberg model with arbitrary spin and range of exchange*, Phys. Rev. **145**, 288 (1966), doi:[10.1103/PhysRev.145.288](https://doi.org/10.1103/PhysRev.145.288).
- [30] H. B. Callen and E. Callen, *Cluster approximation for ferromagnets with first- and second-neighbor exchange, with application to the europium chalcogenides*, Phys. Rev. **136**, A1675 (1964), doi:[10.1103/PhysRev.136.A1675](https://doi.org/10.1103/PhysRev.136.A1675).
- [31] T. Fujishiro, F. Takano and T. Oguchi, *Statistical theory of ferro- and antiferromagnetism*, Journal of the Physical Society of Japan **19**(9), 1666 (1964), doi:[10.1143/JPSJ.19.1666](https://doi.org/10.1143/JPSJ.19.1666), <https://doi.org/10.1143/JPSJ.19.1666>.
- [32] G. An, *A note on the cluster variation method*, Journal of Statistical Physics **52**(3), 727 (1988), doi:[10.1007/BF01019726](https://doi.org/10.1007/BF01019726).
- [33] Y.-L. Wang, C. Wentworth and B. Westwanski, *Linked-cluster expansion for quantum spin systems and the perpendicular susceptibility of the Ising model*, Phys. Rev. B **32**, 1805 (1985), doi:[10.1103/PhysRevB.32.1805](https://doi.org/10.1103/PhysRevB.32.1805).
- [34] C. Wentworth and Y.-L. Wang, *Linked-cluster series-expansion technique for quantum spin systems*, Phys. Rev. B **36**, 8687 (1987), doi:[10.1103/PhysRevB.36.8687](https://doi.org/10.1103/PhysRevB.36.8687).
- [35] C. Wentworth, Y. L. Wang and B. Westwanski, *Linked-cluster series expansion for the spin-one Heisenberg model with easy-axis single-ion anisotropy*, Journal of Physics C: Solid State Physics **20**(36), 6255 (1987), doi:[10.1088/0022-3719/20/36/024](https://doi.org/10.1088/0022-3719/20/36/024).
- [36] M. Rigol, T. Bryant and R. R. P. Singh, *Numerical linked-cluster approach to quantum lattice models*, Phys. Rev. Lett. **97**, 187202 (2006), doi:[10.1103/PhysRevLett.97.187202](https://doi.org/10.1103/PhysRevLett.97.187202).
- [37] M. Rigol, T. Bryant and R. R. P. Singh, *Numerical linked-cluster algorithms. I. spin systems on square, triangular, and kagomé lattices*, Phys. Rev. E **75**, 061118 (2007), doi:[10.1103/PhysRevE.75.061118](https://doi.org/10.1103/PhysRevE.75.061118).
- [38] B. Tang, E. Khatami and M. Rigol, *A short introduction to numerical linked-cluster expansions*, Computer Physics Communications **184**(3), 557 (2013), doi:<https://doi.org/10.1016/j.cpc.2012.10.008>.
- [39] E. Khatami and M. Rigol, *Thermodynamics of the antiferromagnetic Heisenberg model on the checkerboard lattice*, Phys. Rev. B **83**, 134431 (2011), doi:[10.1103/PhysRevB.83.134431](https://doi.org/10.1103/PhysRevB.83.134431).
- [40] R. Applegate, N. R. Hayre, R. R. P. Singh, T. Lin, A. G. R. Day and M. J. P. Gingras, *Vindication of $\text{Yb}_2\text{Ti}_2\text{O}_7$ as a model exchange quantum spin ice*, Phys. Rev. Lett. **109**, 097205 (2012), doi:[10.1103/PhysRevLett.109.097205](https://doi.org/10.1103/PhysRevLett.109.097205).
- [41] F. D. M. Haldane, *Nonlinear field theory of large-spin Heisenberg antiferromagnets: Semiclassically quantized solitons of the one-dimensional easy-axis Néel state*, Phys. Rev. Lett. **50**, 1153 (1983), doi:[10.1103/PhysRevLett.50.1153](https://doi.org/10.1103/PhysRevLett.50.1153).
- [42] I. Affleck, T. Kennedy, E. H. Lieb and H. Tasaki, *Rigorous results on valence-bond ground states in antiferromagnets*, Phys. Rev. Lett. **59**, 799 (1987), doi:[10.1103/PhysRevLett.59.799](https://doi.org/10.1103/PhysRevLett.59.799).
- [43] I. Affleck, T. Kennedy, E. H. Lieb and H. Tasaki, *Valence bond ground states in isotropic quantum antiferromagnets*, Communications in Mathematical Physics **115**(3), 477 (1988).

- [44] D. A. Huse and V. Elser, *Simple variational wave functions for two-dimensional Heisenberg spin- $1/2$ antiferromagnets*, Phys. Rev. Lett. **60**, 2531 (1988), doi:[10.1103/PhysRevLett.60.2531](https://doi.org/10.1103/PhysRevLett.60.2531).
- [45] T. Jolicoeur, E. Dagotto, E. Gagliano and S. Bacci, *Ground-state properties of the $S = 1/2$ Heisenberg antiferromagnet on a triangular lattice*, Phys. Rev. B **42**, 4800 (1990), doi:[10.1103/PhysRevB.42.4800](https://doi.org/10.1103/PhysRevB.42.4800).
- [46] S. R. White and A. L. Chernyshev, *Néel order in square and triangular lattice Heisenberg models*, Phys. Rev. Lett. **99**, 127004 (2007), doi:[10.1103/PhysRevLett.99.127004](https://doi.org/10.1103/PhysRevLett.99.127004).
- [47] A. Honecker, J. Schulenburg and J. Richter, *Magnetization plateaus in frustrated antiferromagnetic quantum spin models*, Journal of Physics: Condensed Matter **16**(11), S749 (2004), doi:[10.1088/0953-8984/16/11/025](https://doi.org/10.1088/0953-8984/16/11/025).
- [48] D. Sellmann, X.-F. Zhang and S. Eggert, *Phase diagram of the antiferromagnetic XXZ model on the triangular lattice*, Phys. Rev. B **91**, 081104 (2015), doi:[10.1103/PhysRevB.91.081104](https://doi.org/10.1103/PhysRevB.91.081104).
- [49] T. Sakai and H. Nakano, *Critical magnetization behavior of the triangular- and kagome-lattice quantum antiferromagnets*, Phys. Rev. B **83**, 100405 (2011), doi:[10.1103/PhysRevB.83.100405](https://doi.org/10.1103/PhysRevB.83.100405).
- [50] J. Richter, J. Schulenburg and A. Honecker, *Quantum magnetism in two dimensions: From semi-classical Néel order to magnetic disorder*, pp. 85–153, Springer Berlin Heidelberg, Berlin, Heidelberg, ISBN 978-3-540-40066-0, doi:[10.1007/BFb0119592](https://doi.org/10.1007/BFb0119592) (2004).
- [51] L. Seabra, T. Momoi, P. Sindzingre and N. Shannon, *Phase diagram of the classical Heisenberg antiferromagnet on a triangular lattice in an applied magnetic field*, Phys. Rev. B **84**, 214418 (2011), doi:[10.1103/PhysRevB.84.214418](https://doi.org/10.1103/PhysRevB.84.214418).
- [52] D. Yamamoto, G. Marmorini and I. Danshita, *Quantum phase diagram of the triangular-lattice XXZ model in a magnetic field*, Phys. Rev. Lett. **112**, 127203 (2014), doi:[10.1103/PhysRevLett.112.127203](https://doi.org/10.1103/PhysRevLett.112.127203).
- [53] D. Yamamoto, G. Marmorini and I. Danshita, *Magnetization process of spin- $1/2$ Heisenberg antiferromagnets on a layered triangular lattice*, Journal of the Physical Society of Japan **85**(2), 024706 (2016), doi:[10.7566/JPSJ.85.024706](https://doi.org/10.7566/JPSJ.85.024706), <https://doi.org/10.7566/JPSJ.85.024706>.
- [54] A. V. Chubukov and D. I. Golosov, *Quantum theory of an antiferromagnet on a triangular lattice in a magnetic field*, Journal of Physics: Condensed Matter **3**(1), 69 (1991), doi:[10.1088/0953-8984/3/1/005](https://doi.org/10.1088/0953-8984/3/1/005).
- [55] A. V. Chubukov and T. Jolicoeur, *Order-from-disorder phenomena in Heisenberg antiferromagnets on a triangular lattice*, Phys. Rev. B **46**, 11137 (1992), doi:[10.1103/PhysRevB.46.11137](https://doi.org/10.1103/PhysRevB.46.11137).
- [56] B. Kleine, E. Müller-Hartmann, K. Frahm and P. Fazekas, *Spin-wave analysis of easy-axis quantum antiferromagnets on the triangular lattice*, Zeitschrift für Physik B Condensed Matter **87**, 103 (1992), doi:[10.1007/BF01308264](https://doi.org/10.1007/BF01308264).
- [57] Q. Sheng and C. L. Henley, *Ordering due to disorder in a triangular Heisenberg antiferromagnet with exchange anisotropy*, Journal of Physics: Condensed Matter **4**(11), 2937 (1992), doi:[10.1088/0953-8984/4/11/020](https://doi.org/10.1088/0953-8984/4/11/020).

- [58] R. Moessner and S. L. Sondhi, *Ising models of quantum frustration*, Phys. Rev. B **63**, 224401 (2001), doi:[10.1103/PhysRevB.63.224401](https://doi.org/10.1103/PhysRevB.63.224401).
- [59] M. A. Nielsen and I. L. Chuang, *Quantum Computation and Quantum Information*, Cambridge University Press, doi:[10.1017/CBO9780511976667](https://doi.org/10.1017/CBO9780511976667) (2010).
- [60] F. Pollmann and A. M. Turner, *Detection of symmetry-protected topological phases in one dimension*, Phys. Rev. B **86**, 125441 (2012), doi:[10.1103/PhysRevB.86.125441](https://doi.org/10.1103/PhysRevB.86.125441).
- [61] Z. Zhu and S. R. White, *Spin liquid phase of the $S = \frac{1}{2} J_1 - J_2$ Heisenberg model on the triangular lattice*, Phys. Rev. B **92**, 041105 (2015), doi:[10.1103/PhysRevB.92.041105](https://doi.org/10.1103/PhysRevB.92.041105).
- [62] W.-J. Hu, S.-S. Gong, W. Zhu and D. N. Sheng, *Competing spin-liquid states in the spin- $\frac{1}{2}$ Heisenberg model on the triangular lattice*, Phys. Rev. B **92**, 140403 (2015), doi:[10.1103/PhysRevB.92.140403](https://doi.org/10.1103/PhysRevB.92.140403).
- [63] Y. Iqbal, W.-J. Hu, R. Thomale, D. Poilblanc and F. Becca, *Spin liquid nature in the Heisenberg $J_1 - J_2$ triangular antiferromagnet*, Phys. Rev. B **93**, 144411 (2016), doi:[10.1103/PhysRevB.93.144411](https://doi.org/10.1103/PhysRevB.93.144411).
- [64] A. Wietek and A. M. Läuchli, *Chiral spin liquid and quantum criticality in extended $S = \frac{1}{2}$ Heisenberg models on the triangular lattice*, Phys. Rev. B **95**, 035141 (2017), doi:[10.1103/PhysRevB.95.035141](https://doi.org/10.1103/PhysRevB.95.035141).
- [65] S. Hu, W. Zhu, S. Eggert and Y.-C. He, *Dirac spin liquid on the spin-1/2 triangular Heisenberg antiferromagnet*, Phys. Rev. Lett. **123**, 207203 (2019), doi:[10.1103/PhysRevLett.123.207203](https://doi.org/10.1103/PhysRevLett.123.207203).
- [66] S.-S. Gong, W. Zheng, M. Lee, Y.-M. Lu and D. N. Sheng, *Chiral spin liquid with spinon Fermi surfaces in the spin- $\frac{1}{2}$ triangular Heisenberg model*, Phys. Rev. B **100**, 241111 (2019), doi:[10.1103/PhysRevB.100.241111](https://doi.org/10.1103/PhysRevB.100.241111).
- [67] Y.-F. Jiang and H.-C. Jiang, *Nature of quantum spin liquids of the $S = \frac{1}{2}$ Heisenberg antiferromagnet on the triangular lattice: A parallel DMRG study*, Phys. Rev. B **107**, L140411 (2023), doi:[10.1103/PhysRevB.107.L140411](https://doi.org/10.1103/PhysRevB.107.L140411).
- [68] M. den Nijs and K. Rommelse, *Preroughening transitions in crystal surfaces and valence-bond phases in quantum spin chains*, Phys. Rev. B **40**, 4709 (1989), doi:[10.1103/PhysRevB.40.4709](https://doi.org/10.1103/PhysRevB.40.4709).
- [69] Y. Da Liao, H. Li, Z. Yan, H.-T. Wei, W. Li, Y. Qi and Z. Y. Meng, *Phase diagram of the quantum Ising model on a triangular lattice under external field*, Phys. Rev. B **103**, 104416 (2021), doi:[10.1103/PhysRevB.103.104416](https://doi.org/10.1103/PhysRevB.103.104416).
- [70] S. R. White and R. M. Noack, *Real-space quantum renormalization groups*, Phys. Rev. Lett. **68**, 3487 (1992), doi:[10.1103/PhysRevLett.68.3487](https://doi.org/10.1103/PhysRevLett.68.3487).
- [71] M. Fishman, S. R. White and E. M. Stoudenmire, *Codebase release 0.3 for ITensor*, SciPost Phys. Codebases pp. 4–r0.3 (2022), doi:[10.21468/SciPostPhysCodeb.4-r0.3](https://doi.org/10.21468/SciPostPhysCodeb.4-r0.3).
- [72] M. C. Gutzwiller, *Correlation of electrons in a narrow s band*, Phys. Rev. **137**, A1726 (1965), doi:[10.1103/PhysRev.137.A1726](https://doi.org/10.1103/PhysRev.137.A1726).
- [73] W. Metzner and D. Vollhardt, *Analytic calculation of ground-state properties of correlated fermions with the Gutzwiller wave function*, Phys. Rev. B **37**, 7382 (1988), doi:[10.1103/PhysRevB.37.7382](https://doi.org/10.1103/PhysRevB.37.7382).

- [74] X. Deng, L. Wang, X. Dai and Z. Fang, *Local density approximation combined with Gutzwiller method for correlated electron systems: Formalism and applications*, Phys. Rev. B **79**, 075114 (2009), doi:[10.1103/PhysRevB.79.075114](https://doi.org/10.1103/PhysRevB.79.075114).
- [75] N. Lanatà, H. U. R. Strand, X. Dai and B. Hellsing, *Efficient implementation of the Gutzwiller variational method*, Phys. Rev. B **85**, 035133 (2012), doi:[10.1103/PhysRevB.85.035133](https://doi.org/10.1103/PhysRevB.85.035133).
- [76] T. Ayral, T.-H. Lee and G. Kotliar, *Dynamical mean-field theory, density-matrix embedding theory, and rotationally invariant slave bosons: A unified perspective*, Phys. Rev. B **96**, 235139 (2017), doi:[10.1103/PhysRevB.96.235139](https://doi.org/10.1103/PhysRevB.96.235139).
- [77] C. Schilling, *The quantum marginal problem*, <https://arxiv.org/abs/1404.1085>.
- [78] X.-D. Yu, T. Simnacher, N. Wyderka, H. C. Nguyen and O. Gühne, *A complete hierarchy for the pure state marginal problem in quantum mechanics*, Nature Communications **12**(1), 1012 (2021), doi:[10.1038/s41467-020-20799-5](https://doi.org/10.1038/s41467-020-20799-5).
- [79] G. Biroli, O. Parcollet and G. Kotliar, *Cluster dynamical mean-field theories: Causality and classical limit*, Phys. Rev. B **69**, 205108 (2004), doi:[10.1103/PhysRevB.69.205108](https://doi.org/10.1103/PhysRevB.69.205108).
- [80] A. J. Guttmann, *Phase transitions and critical phenomena*, edited by C. Domb and M. S. Green, vol. 13, Academic Press, London (1989).
- [81] W. H. Press, B. P. Flannery, S. A. Teukolsky and W. T. Vetterling, *Numerical Recipes in Fortran: (Cambridge University Press, 1999)*, Cambridge University Press (1999).